11-15-2013

Development of a Coupling Model for Fluid-Structure Interaction using the Mesh-free Finite Element Method and the Lattice Boltzmann Method

Jaime Mudrich
Florida International University, jmudr001@fiu.edu

FLORIDA INTERNATIONAL UNIVERSITY

Miami, Florida

DEVELOPMENT OF A COUPLING MODEL FOR FLUID-STRUCTURE INTERACTION USING THE MESH-FREE FINITE ELEMENT METHOD AND THE LATTICE BOLTZMANN METHOD

A thesis submitted in partial fulfillment of the

requirements for the degree of

MASTER OF SCIENCE

in

MECHANICAL ENGINEERING

by

Jaime Mudrich

2013

To: Dean Amir Mirmiran
College of Engineering and Computing

This thesis, written by Jaime Mudrich, and entitled Development of a Coupling Model for Fluid-Structure Interaction using the Mesh-free Finite Element Method and the Lattice Boltzmann Method, having been approved in respect to style and intellectual content, is referred to you for judgment.

We have read this thesis and recommend that it be approved.

George Dulikravich

Michael Sukop

Leonel Lagos

Igor Tsukanov, Major Professor

Date of Defense: November 15, 2013

The thesis of Jaime Mudrich is approved.

Dean Amir Mirmiran
College of Engineering and Computing

Dean Lakshmi N Reddi
University Graduate School

Florida International University, 2013

ACKNOWLEDGMENTS

I would like to thank Dr. Leonel Lagos, the Program Director of the United States DOE/FIU Science and Technology Workforce Development Initiative which has in part supported this research. Dr. Lagos has been vigilant in providing students like myself opportunities to work with experienced Research Scientists on challenging projects, refining professional and academic skills all the while. *Ganas...*

I would like to thank Dr. Seckin Gokaltun, my mentor during my time as a Department of Energy Fellow, for inspiring me to study the lattice Boltzmann method which has become a cornerstone of my graduate career. He has always encouraged me to take on new tasks of which I had no experience and provided limitless support through their completion, resulting in continuous learning and growth.

I would like to thank Dr. Igor Tsukanov, my major professor during my graduate career, for piquing my interest in computational mechanics as an undergraduate student. I have found Dr. Tsukanov to be a great role model for my academic career. He is a brilliant educator, capable of communicating the most abstract of ideas in a manner which provides fundamental understanding while never losing site of pragmatic value. I would also like to thank him, of course, for his extensive support in the preparation of this thesis research.

I would like to thank the remaining members of my thesis committee, Dr. George Dulikravich and Dr. Michael Sukop, not only for service on my thesis committee, but for their individual contributions to my academic career. Dr. Dulikravich for his powerful, broad and enthusiastic lectures on fluid mechanics which have prepared me well for this research and future engineering endeavors. Dr. Sukop for in-depth lattice Boltzmann method education and exposing me to the real power of the method via his striking research in simulating multiphase fluid flow through porous media.

ABSTRACT OF THE THESIS

DEVELOPMENT OF A COUPLING MODEL FOR FLUID-STRUCTURE INTERACTION USING THE MESH-FREE FINITE ELEMENT METHOD AND THE LATTICE BOLTZMANN METHOD

by

Jaime Mudrich

Florida International University, 2013

Miami, Florida

Professor Igor Tsukanov, Major Professor

In the presented thesis work, the meshfree method with distance fields was coupled with the lattice Boltzmann method to obtain solutions of fluid-structure interaction problems. The thesis work involved development and implementation of numerical algorithms, data structure, and software. Numerical and computational properties of the coupling algorithm combining the meshfree method with distance fields and the lattice Boltzmann method were investigated. Convergence and accuracy of the methodology was validated by analytical solutions.

The research was focused on fluid-structure interaction solutions in complex, mesh-resistant domains as both the lattice Boltzmann method and the meshfree method with distance fields are particularly adept in these situations. Furthermore, the fluid solution provided by the lattice Boltzmann method is massively scalable, allowing extensive use of cutting edge parallel computing resources to accelerate this phase of the solution process. The meshfree method with distance fields allows for exact satisfaction of boundary conditions making it possible to exactly capture the effects of the fluid field on the solid structure.

TABLE OF CONTENTS

CHAPTER PAGE

1 INTRODUCTION 1
1.1 Motivation 2
1.2 Problem Description 4
1.3 Literature Survey 5
1.4 Proposal 7
1.5 Personal Contribution 7

2 NUMERICAL FORMULATION 9
2.1 Lattice Boltzmann Method 9
2.1.1 Single Relaxation-Time 11
2.1.2 D2Q9 lattice 12
2.2 Meshfree FEM with Distance Fields 13
2.3 Coupling Algorithm 15

3 NUMERICAL EXPERIMENTS 20
3.1 FSI Model Verification 20
3.1.1 Lattice Boltzmann Method Verification 20
3.1.2 Coupling Method and Meshfree Method Verification 23
3.2 Convergence of the Interpolation Algorithm at Solid-Fluid Interface 27
3.3 Demonstration Case 1: Flow through a restricted channel 32
3.4 Demonstration Case 2: Flow past an irregular body. 35

4 DISCUSSION AND CONCLUSION 39

5 APPENDICES 41

REFERENCES 46

LIST OF FIGURES

FIGURE PAGE

2.1 Geometry of an organ with a tesselated surface representation. 10

2.2 Geometry of an organ with a voxelized volumetric representation. 10

2.3 The two-dimensional, nine component lattice. (D2Q9) 12

2.4 Representation of LBM domain that is to be treated by coupling method before being transferred to the solid solver. 16

2.5 Boundary values used in the meshfree method with distance fields are extracted from the LBM fluid field via bilinear interpolation. 17

2.6 Each row is first interpolated individually, only including fluid nodes. Solid nodes are then populated from the interpolation value at their location. 18

2.7 Each column is interpolated individually, only including fluid nodes. Solid nodes are then populated from the average of the column-interpolation value and row-interpolation value at the solid node location. 19

3.1 Fluidic problem description using physical units. 21

3.2 Fluidic problem description using non-dimensional lattice units. 22

3.3 Pressure field from fluid component of verification. Legend units are in Pascals. Black border represents solid, inactive portion of domain. 23

3.4 Analytical model for structural problem for meshfree method with distance fields verification. 24

3.5 Displacement results from meshfree method with distance fields using LBM-generated pressure field and passed using the coupling method described in section 2.3. 25

3.6 Displacement results from Solidworks Simulation, applying a linear increasing pressure boundary condition representing the hydrostatic fluid pressure load. 26

3.7 Convergence experiment setup 28

3.8 Functions used to test convergence. 28

3.9 Test point evaluation procedure. 29

3.10 Polynomial convergence on circle. 30

3.11 Polynomial convergence on cross. 31

3.12 Ellipse convergence on circle. 32
3.13 Impeded Channel Velocity Field. 34
3.14 Impeded Channel Pressure Field. 34
3.15 Impeded Channel Structural Analysis. 34
3.16 Sketch of irregular immersed body. 36
3.17 Velocity field around irregular body. 36
3.18 Pressure field around irregular body. 37
3.19 Displacement of irregular body. 37
3.20 Channel-induced stress on irregular body. 38

5.1 Cross-sectional dimensions of beam used in structural analysis. 43
5.2 Ellipse convergence on cross. 43
5.3 Trig function convergence on circle. 44
5.4 Trig function convergence on cross. 45

CHAPTER 1

INTRODUCTION

Computational physics is a powerful tool for today's engineer. It allows for tremendous financial and temporal savings in various scientific fields. In design, accurate simulation enables more viable prototypes and hastens the iterative design process. In research, simulation can facilitate experimentation by providing a starting point for investigation, saving valuable research resources. Moreover, computational physics can even aid in investigating phenomena for which experimentation is not possible, such as events taking place over a long period of time like climate change.

Some examples of regularly simulated phenomena are heat transfer, electro-magnetics, fluid dynamics and structural analysis. There are also cases when these phenomena interact with one another and are simulated together. Of particular interest is the coupling of fluid dynamics with structural analysis to model fluid-structure interaction (FSI), the focus of this study. Examples of FSI in engineering include aircraft wings, turbine blades, bridges, artificial heart valves and watercrafts.

The study of fluid dynamics, in particular, greatly benefits from simulation. The most popular and complete fluid dynamics model used for simulation is the Navier-Stokes equations (NSE). The NSE are a set of nonlinear partial differential equations [(1.1), (1.2), and (1.3)] that are impervious to analytical solution without significant, and often impermissible, simplifying assumptions. To overcome the complexity of the equations, numerical solutions are used that make extensive use of advanced computational resources. Doing so allows for accurate simulations of various phenomena such as boundary layer development, chemically reactive flows and shock waves in supersonic fluid flow. One drawback of numerical solutions to the Navier-Stokes equations is that the solution method typically requires a body-fitted mesh. Another drawback is that the pressure-velocity type computational methods for solving the NSE require the solution of the elliptic pressure Poisson equation. This is a drawback because the elliptic nature of the pressure Poisson equation requires an iterative solution and substantial global communications in parallel simulations, adversely affecting scalability.

$$\frac{\partial \rho}{\partial t} + \nabla \cdot (\rho \overrightarrow{V}) = \dot{m} \tag{1.1}$$

$$\frac{\partial (\rho \overrightarrow{V})}{\partial t} + \nabla \cdot (\rho \overrightarrow{V} \overrightarrow{V} - T) = \rho \overrightarrow{b} \tag{1.2}$$

$$\frac{\partial (\rho e_0)}{\partial t} + \nabla \cdot (\rho e_0 \overrightarrow{V} - T \cdot \overrightarrow{V} + \dot{\overrightarrow{q_c}} + \dot{\overrightarrow{q_r}}) = \rho \overrightarrow{V} \cdot \overrightarrow{b} + \rho \dot{q} \tag{1.3}$$

In equations (1.1), (1.2) and (1.3), the nomenclatures is as follows. ρ represents density. t represents time. ∇ is the del operator. $\overrightarrow{V}$ represents velocity. $\dot{m}$ represents the rate of generation of mass per unit time per unit volume. T is the Cauchy stress tensor. $\overrightarrow{b}$ is a body-force-generated acceleration. e_0 is specific total energy. $\dot{q}$ is the time rate of internal heat generation per unit volume. $\dot{\overrightarrow{q_c}}$ is the conduction heat transfer flux and $\dot{\overrightarrow{q_r}}$ is the radiative heat transfer flux.

A central challenge to simulations in the aforementioned field is discretization of the computational domain. This process is commonly known as meshing. Meshing is a complicated procedure that is most often performed automatically in contemporary computer-aided engineering (CAE) software. Unfortunately even the best meshing algorithms will fall short with complex and/or relatively small geometric features, requiring a simplified version of the original domain. The removal of these "mesh-resistant" features can result in critical geometric inaccuracies that will contaminate the solution. References providing an overview of meshing deficiencies [1] and of contemporary meshing technology [2] have been included.

With rapid advancement in computational science, particularly parallel computing, simulation is beginning to play an increasingly significant role in research and engineering. As such, it is important to have software based on an accurate physical model that is capable of simulating a variety of complex physical behavior. Additionally, it is important that the model be able to make efficient use of cutting edge parallel computing resources.

1.1 Motivation

The motivation for this research comes from three major ideas. The first is that fluid-structure interaction simulations can provide valuable insight into a variety of phys-

ical phenomena. One instance is the start-up and shut-down phases of a rocket engine. During start-up, a blast wave traverses the entire nozzle initiating flow. While the nozzle is typically axisymmetric, the transient flow during start-up and shut-down may not exhibit the same symmetry and result in side loading. Simulation of this phenomena enables understanding of stress and deformation induced by the flow on the nozzle and the reaction on the flow itself. Such understanding allows for more robust design that simultaneously maintains both the structural integrity of the flow and of the nozzle. Another phenomena that is better understood through the study of fluid-structure interaction is blood flow through an elastic vessel [3]. As blood is pumped through the body, blood vessels will expand and contract accordingly. Simulation of this phenomena can facilitate in the design of stents which are implanted into blood vessels to keep them from becoming blocked. Another simulated phenomena is particulate transport. An example of this is the use of pulsed-air mixing in radioactive waste tanks to promote homogeneity in fluid transport.

The second major concept driving this research is the set of advantages provided with the meshfree finite element method with distance fields. It is not uncommon in the field of fluid-structure interaction to see structures with complex geometric models exhibiting large deformations. In traditional finite element analysis, the aforementioned phenomena might require an unacceptably fine, body-conforming mesh to represent the complex geometry and recreation of this mesh at every time step during integration to accommodate large deformations. The meshfree finite element method with distance fields [1] employed in this research does not require a mesh that conforms to the geometric representation of the simulation domain and so readily accepts complex geometries. Additionally, robust handling of deforming domains using this methodology has already been demonstrated[4]. The meshfree method with distance fields is also capable of satisfying complex boundary conditions exactly. This is ideal for application to simulation in domains that extract boundary conditions from a non-analytical fluid field. Exact satisfaction of boundary conditions also causes faster convergence of the approximate solution [4].

The third incentivizer is the robust simulation capabilities of the lattice Boltzmann method as a computational fluid dynamics algorithm. Despite being a young concept (relative to the NSE), the LBM has demonstrated the ability to simulate a large variety of fluid dynamics phenomena with straightforward implementation. LBM simulation was successfully used in computations of shallow flows [5], solute transport [6], multiphase flow [7], cavitation in homogeneous and heterogeneous multiphase fluid [8], turbulence modeling in two-dimensional cavity flow [9], turbulence modeling in three-dimensional pipe flow [10] and non-Newtonian fluid flow [11]. Fluid dynamics simulations in porous media have also been conducted using the LBM [12]. With such versatility as well as massive parallel computation scalability and robust handling of complex geometries, the LBM is not only a desirable fluid mechanics tool, but when paired with structural analysis, can accomplish tremendously complicated FSI simulations all the while utilizing the power of parallel super computers.

1.2 Problem Description

The problem addressed in this research is the computational expense in fluid-structure interaction simulations with complex domains. Employing body-fitting meshes for both the structural solution method and the fluid method in analysis of complex domains requires a very fine mesh that must be regenerated with every time step during integration. This expense is often mitigated by substituting the complex domain with a more simplified domain. This simplification can remove critical features that would impact results and is often impermissible. Another way this computational expense can be relieved is by employing parallel computing resources. An issue with pressure-velocity parallel solution to the NSE is that it requires an iterative solution to the elliptic Poisson pressure equation (PPE). The iterative solution of the PPE requires global communication amongst the parallel computer cluster as opposed to processors only communicating with nearest neighbors. This negatively affects scalability. Another problem with FSI in complex domains is the difficulty in satisfying the complex, non-analytical boundary conditions presented by the interface between the solid and fluid domains. Apart from numerical loss in the process of coupling the two solvers, there will be some natural discretization error in each of the individual fluid and structural numerical methods.

The methodology presented in this thesis aims to increase scalability, facilitate handling of complex geometries and exactly satisfy boundary conditions imposed on to the solid body in fluid structure interaction simulations.

1.3 Literature Survey

Much research has been conducted in the field of FSI simulation. The two dominant approaches for simulating this phenomena are the monolithic and partitioned methodologies. Monolithic methods solve the fluid and structure governing equations simultaneously, employing a single solver. The partitioned approach solves the fluid and structure equations independently and requires a coupler to transfer field data at every time step. Partitioned approaches are by far preferred over monolithic approaches, owed to the preservation of modularity in the solver for each phase. Preservation of this modularity allows for the most efficient solver to be selected for both the structural and the fluid components of the simulation [13], [14].

The immersed boundary method [15] provides one solution for meshfree fluid-structure interaction simulations. This method was originally introduced by Peskin [16] to simulate cardiac mechanics and associated blood flow. In this method, a cartesian mesh serves as the basis for integration instead of a body-fitted mesh. The simplicity afforded by the Cartesian mesh volume representation is balanced by the expense in imposing boundary conditions over the immersed body. One way this is overcome is by adjusting the governing equation (NSE). This typically entails adding a forcing term to the continuous governing equation, with the new equation discretized over the entire domain. The main advantage of the immersed boundary method is that conforming-mesh generation costs are eliminated. This is particularly useful in the case where the body is moving through the fluid domian. The cartesian mesh is unaffected while only the body is displaced and deformed. Two disadvantages of the immersed boundary method are the requirement that the governing equation is modified to impose boundary conditions, and that the governing equation is typically the Navier-Stokes Equation. The method which is the subject of this research does not utilize the NSE and thereby avoids the possible iterative solution of the pressure Poisson equation requiring global communication in parallel computing. Additionally, the proposed method satisfies the

boundary conditions automatically, with no additional effort, and satisfies them exactly, per the benefits of the meshfree method with distance fields [1].

The application of the lattice Boltzmann method in fluid-structure interaction simulation has been explored in several papers. The lattice Boltzmann method was coupled with the finite element method to simulate 3D fluid-structure interaction using the distributed Lagrange multiplier/fictitious domain method (LBM-DLM/FD) [17] . In the LBM-DLM/FD method, the LBM is used to solve the fluid field and the solid domain is filled with a fluid to simplify the fluid boundary geometry. The distributed Lagrange multiplier is used to impose a kinematic constraint on the fictitious-fluid-filled solid domain. Although this method accomplishes 3D FSI simulation using the lattice Boltzmann method, it still requires a body-fitted mesh and depends on the Lagrangian multiplier to constrain velocities in the fictitious fluid.

The lattice Boltzmann method was again coupled with a high-order Finite Element structural discretization [18]. The author takes a partitioned approach employing three separate software components. One is used for the LBM solution, a second for the structural solution, and finally a communication library for coupling the two. The coupling algorithm is primarily built on introducing a moving surface mesh at the interface of the fluid LBM domain and the solid finite element domain. Interface parameters such as velocities and load vectors are passed from the respective solvers to the interface mesh. The interface mesh then distributes these parameters across to the receiving solver. This approach is shown to be accurate through validation against an experimental study of a flag-like structure submerged in an incompressible laminar flow field. While an exceptional approach to fluid-structure interaction simulation using the lattice Boltzmann method, there is still dependence on body-fitted meshing for the structural analysis as well as the maintenance of an interface mesh as the structure deforms.

To the best of the authors knowledge, research in meshfree FSI has yet to couple the LBM with the meshfree method with distance fields. This particular configuration would enjoy benefits such as massive scalability in the fluid dynamics solution, exact satisfaction of boundary conditions in the solid structure solution, and FSI in highly complex geometries such as porous media or organic scans and straightforward expansion

of the fluid solver to include multiple fluid components and phases in the LBM simulation (i.e. oil-water, water-vapor).

1.4 Proposal

This research proposes to demonstrate the feasibility of coupling the LBM with the meshfree method with distance fields as a fluid-structure interaction model. In this study, numerical and computational properties of the proposed approach are investigated. The research considers fluid-solid interaction simulations in two dimensions. The fluid simulations are restricted to steady, low Mach number (per LBM limitations), laminar, isothermal, adiabatic fluid flow. The fluid simulations use a viscous, isotropic, Newtonian fluid model. The structural analysis is confined to small, elastic deformations of isotropic material. The model used does not consider any nonlinearities i.e. geometric, loading, material, etc. With the exception of the low Mach number constraint, these restrictions are imposed merely to focus the research on the coupling algorithm for the proposed FSI method instead of the physics of the individual fluid and structural solution methods. The coupling method is extendable to simulations of three-dimensions and a multitude of fluid and solid models derived from the LBM and meshfree method with distance fields, respectively.

1.5 Personal Contribution

To conduct this research, a model for the coupling of the LBM and the meshfree method with distance fields for fluid-solid interaction simulation was developed. This largely consisted in developing a methodology for mapping physical parameters from the LBM with a discrete domain representation to the meshfree method with distance fields which requires a continuous representation of boundary conditions. After theoretical development, the coupling method was programmed in C++ and verified via interpolation of various analytical functions over arbitrary domains. The research investigated the convergence characteristics of the interpolation/extrapolation scheme by varying the mesh density during coupling and monitoring the maximum error between the interpolated field and the exact, analytical field. Fluid-structure interaction verification simulations were conducted using the developed coupling model to understand its accuracy as a FSI solution method. Upon verification, FSI simulations were

conducted around semi-complex geometries to illustrate the benefits achieved by the proposed meshfree FSI method.

CHAPTER 2

NUMERICAL FORMULATION

2.1 Lattice Boltzmann Method

The lattice Boltzmann method is a computational fluid dynamics method that predicts macroscopic fluid behavior based on the analysis of mesoscopic fluid interaction. Instead of solving the Navier-Stokes equations directly, the LBM provides a basis for numerical solution of the *discrete Boltzmann equation.* The dominant benefits of the method are massive scalability in computational solutions and robust handling of complex domains. Additional points of attraction include the ability to simulate solute transport, multiphase flow and convective heat transfer.

The LBM is massively scalable relative to pressure-velocity type NSE methods due to the fact that density and pressure are related through an equation of state in the LBM. Since pressure can be directly determined from density, there is no need to solve the elliptic Poisson pressure equation. The elliptical nature of the Poisson pressure equation requires iterative solution and substantial global communication in NSE-based, pressure-velocity type fluid dynamics solution methods. Such communication weighs heavily on overall computation speed in the parallel solution of the NSE. Unlike the NSE, the LBM relies exclusively on nearest-neighbor information, only requiring communication of values at the intersection of subdomains [19].

Another advantage of LBM in fluid dynamics simulation is robust handling of complex geometries. The lattice Boltzmann method does not require a body-fitted mesh as in most contemporary NSE solvers, but instead employs a structured, Cartesian lattice. Each node is designated as either a solid or fluid and treated accordingly. Solid nodes at the fluid-solid interface are subject to the bounce-back boundary condition [20], satisfying the no-slip, zero velocity boundary condition. Furthermore, it is possible to easily convert digital scans into voxelized representations ready for use with the LBM [21], simulating flow through porous media. Figure 2.1 depicts a surface representation of a human organ suitable for visualization, but not for simulation. Figure 2.2 illustrates a volumetric, voxelized representation of the same organ presented in figure 2.1. In a LBM simulation, the voxels may be designated as solid or fluid and are automatically

treated using the bounce-back boundary condition.

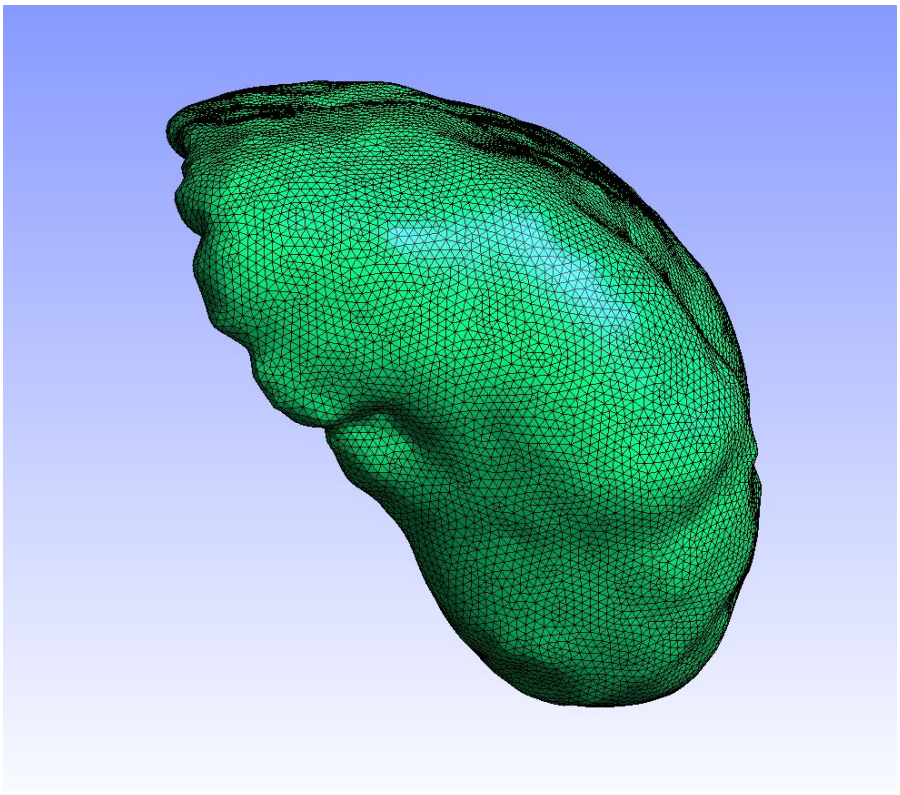

Figure 2.1: Geometry of an organ with a tesselated surface representation.

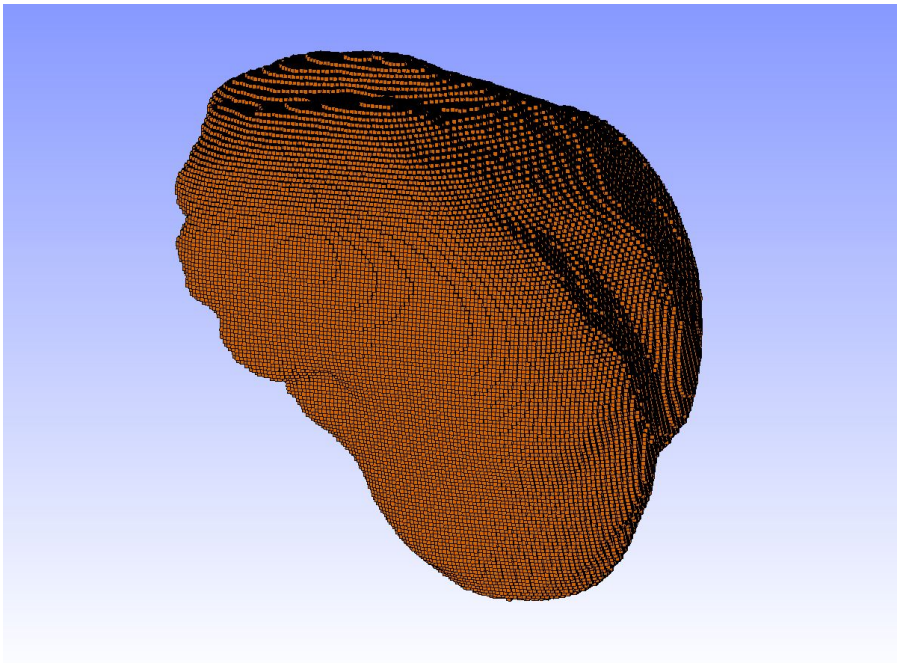

Figure 2.2: Geometry of an organ with a voxelized volumetric representation.

2.1.1 Single Relaxation-Time

The single relaxation-time LBM model, also known as the Bhatnagar-Gross-Krook (BGK) model [22] is the simplest form of the lattice Boltzmann method. The BGK model employs only one relaxation time as opposed to the multiple-relaxation-time model [23]. The multiple-relaxation-time model has been shown to be more stable, but with added computational expense. The simplicity of the BGK model makes it appropriate for this FSI model presented here. In future work it may be desirable to incorporate a multiple-relaxation-time model. Equations (2.1) through (2.10) to follow are taken from an introductory text to the lattice Boltzmann method [24].

Equation (2.1) below expresses the discrete lattice Boltzmann equation using the BGK collision operator. In this equation, f_i represents the i^{th} component of the density distribution function. $\overrightarrow{e}_i$ represents the discrete velocity component in the i^{th} direction. $\overrightarrow{x}$ represents the position vector. t represents time. δt represents a change in time step and is set equal to unity in this research. τ represents relaxation time. ${f_i}^{eq}$ represents the equilibrium value of the i^{th} component of the density distribution function.

$$f_i(\overrightarrow{x} + \overrightarrow{e}_i\delta t, t + \delta t) = f_i(\overrightarrow{x}, t) + \frac{1}{\tau}({f_i}^{eq} - f_i) \tag{2.1}$$

The left-hand side of Equation (2.1) is an advection or "streaming" step where the i^{th} component of the density distribution function is streamed to the nearest neighbor in the i^{th} direction. The right-hand side of this equation is a collision step where the density distribution function is relaxed to its equilibrium value. Equation (2.2) is used for calculation of the equilibrium density distribution. In Equation (2.2), w_i represents a direction specific weighting coefficient. ρ represents macroscopic density. $\overrightarrow{u}$ represents macroscopic velocity. c represents the lattice speed as expressed in Equation (2.3). In Equation (2.3), δx is the distance between lattice units and is set to unity for this research, resulting in $c = 1$.

$${f_i}^{eq}(\overrightarrow{x}) = w_i\rho(\overrightarrow{x})[1 + 3\frac{\overrightarrow{e}_i \cdot \overrightarrow{u}}{c^2} + \frac{9}{2}\frac{(\overrightarrow{e}_i \cdot \overrightarrow{u})^2}{c^4} - \frac{3}{2}\frac{\overrightarrow{u} \cdot \overrightarrow{u}}{c^2}] \tag{2.2}$$

$$c = \frac{\delta x}{\delta t} \tag{2.3}$$

To obtain the macroscopic density and velocity, Equation (2.4) and Equation (2.5) are used, respectively. In these equations, n represents the number of discrete components pertaining to the lattice in use. Pressure is then calculated using Equation (2.6) in which c_s represents the lattice speed of sound and expressed in Equation (2.7).

$$\rho = \sum_{i=0}^{n} f_i \tag{2.4}$$

$$\overrightarrow{u} = \frac{1}{\rho} \sum_{i=0}^{n} f_i \overrightarrow{e}_i \tag{2.5}$$

$$p = c_s^2 \rho \tag{2.6}$$

$$c_s = \frac{c}{\sqrt{3}} \tag{2.7}$$

2.1.2 D2Q9 lattice

To utilize the lattice Boltzmann method, the density distribution function must be discretized at each node. The discretization used for this research is denoted D2Q9, meaning *two* dimensional lattice with *nine* components of the distribution function. The D2Q9 discretization is illustrated in figure 2.3. In this figure, the vector values of the ve-

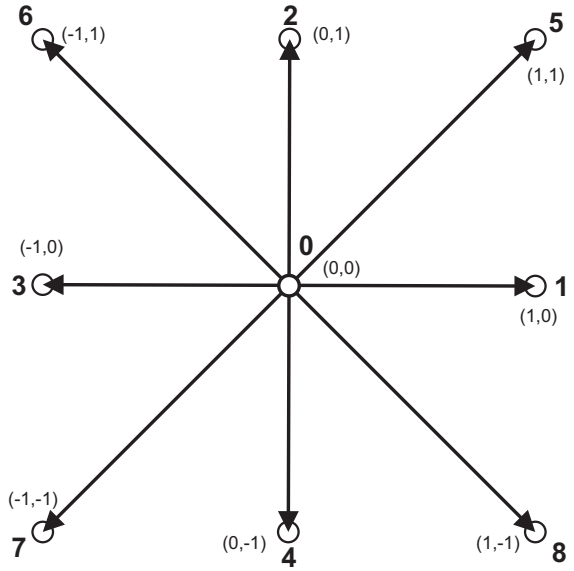

Figure 2.3: The two-dimensional, nine component lattice. (D2Q9)

locity components are expressed as an ordered pair pointing towards neighboring nodes. The discrete velocity components are explicitly defined by Equation (2.8). Equation (2.9) defines w_i for this discretization which was earlier used in Equation (2.2). Finally, using the D2Q9 lattice, the kinematic viscosity of the simulated fluid is defined by Equation (2.10). $\tau > 1/2$ is required for positive (physical) viscosity; numerical difficulties emerge as τ approaches $1/2$ [24]. A value of $\tau = 1$ is commonly suggested and is used in this research, yielding a viscosity of $\nu = 1/6$. Other common discretizations are the D2Q5 and, in three dimensions, the D3Q15, D3Q19 and D3Q27.

$$\overrightarrow{e_i} = \begin{cases} (0,0) & i = 0 \\ (1,0),(0,1),(-1,0),(0,-1) & i = 1,2,3,4 \\ (1,1),(-1,1),(-1,-1),(1,-1) & i = 5,6,7,8 \end{cases} \tag{2.8}$$

$$w_i = \begin{cases} 4/9 & i = 0 \\ 1/9 & i = 1,2,3,4 \\ 1/36 & i = 5,6,7,8 \end{cases} \tag{2.9}$$

$$\nu = c_s^2(\tau - \frac{1}{2}\delta t) \tag{2.10}$$

2.2 Meshfree Finite Element Method with Distance Fields

At the core of the meshfree method of analysis with distance fields is the representation of a physical field by the Taylor series expansion, originally proposed by Kantorovich [25] and developed by Rvachev [26, 27]:

$$u(\omega) = u(0) + \sum_{k=1}^{m} \frac{1}{k!} u_k(0)\omega^k + \omega^{k+1}\Phi. \tag{2.11}$$

This representation is a straightforward generalization of a classical Taylor series, where the term $|x - x_o|$, measuring the distance to the point x_o, is replaced by ω measuring the distance to a set of points. Similarly, the kth order derivatives of the function u in the classical Taylor series are replaced by coefficients u_k that are kth order derivatives

of the function u in the direction n normal to the boundary of a geometric domain. In contrast with classical Taylor series, where the coefficients are constants, $u_k(x, y, z)$ in the expression (2.11) may be arbitrary functions. This also holds when ω represents *approximate* distance to the geometric boundary. Taylor series (2.11) provides connection between the value of a physical field at any spatial point and values of the field and its normal derivatives prescribed on the boundary of a geometric domain. In the context of engineering analysis this means that the function u given by expression (2.11) satisfies specified boundary conditions *exactly*.

The remainder term $\omega^{k+1}\Phi$ assures completeness of the Taylor series [27], and it can be used to satisfy additional constraints imposed on u, which are usually formulated in the form of differential equations, integral equations, or variational principles. To find a function u that satisfies both boundary conditions and additional constraints one needs to determine the function Φ. In most cases, this problem has no exact solution. Thus, Φ is approximated by linear combination of basis functions:

$$\Phi = \sum_{i=1}^{N} C_i \chi_i. \tag{2.12}$$

Now, the solution of the original problem is transformed into determining the numerical values of the coefficients C_i in expression (2.12) by *any* standard numerical method. The basis functions χ_i in the last expression can be chosen from any sufficiently complete system of linearly independent functions: polynomials, radial basis functions, B-splines or even finite elements.

Representing physical fields by Taylor series (2.11) reveals two salient features of the meshfree method: exact treatment of boundary conditions (this is the only meshfree method which allows exact treatment of different types of boundary conditions), and clean and modular separation of geometric and analytic information [4]. The shape of the geometric domain is completely described by distance ω to the boundary; and the basis functions can be defined on a mesh that does not conform to the geometric input. Time varying geometric models in particular benefit from this streamlining when the traditional alternative is remeshing with every change in geometry [4].

Using the meshfree method with distance fields, fully automated analyses for a variety of engineering problems and boundary conditions starting with the standard geometric representations have been demonstrated [28, 29]. These include thermal, structural, fluid flow, and many other types of problems. Since a physical field u represented by Expression (2.11) satisfies the prescribed boundary conditions exactly, the solution procedure needs to determine numerical values of the coefficients C_i in the remainder term (2.12) such that u gives the best approximation to the differential equation of the problem. A typical solution procedure includes construction of distance fields to the boundaries where boundary conditions are specified, differentiation of the functions in the Taylor series (2.11) with respect to spatial coordinates, integration over the un-meshed geometric domain and its boundary, solution of an algebraic problem, and visualization of the analysis results.

2.3 Model for Coupling the LBM and Meshfree Finite Element Method with Distance Fields

For the fluid field and solid structure to interact with one another, it is necessary to be able to transfer results from each step of either solution method to the other for the FSI simulation to progress. This procedure may be straightforward in a monolithic approach where both balance equations are solved simultaneously. However, the more common case is the partitioned approach, whereby two independent methodologies are used; one for each phase. Utilization of independent solution methodologies allows for different representations of the solid-fluid interface, preventing direct transfer of the boundary state. In this research, the fluid solution algorithm, LBM, employs a discrete volumetric representation of the solid-fluid interface. The meshfree method with distance fields, however, represents the solid-fluid boundary exactly, with no discretization. Figure 2.4 provides an overlay of the continuous, exact representation by the meshfree method with distance fields (gray potato) and the discrete representation by the LBM. At each node, the LBM requires a binary piece of information indicating whether the node is to be treated as a solid or as a fluid. In Figure 2.4, the empty circles represent fluid nodes whereas the filled in circles within the gray potato indicate solid nodes.

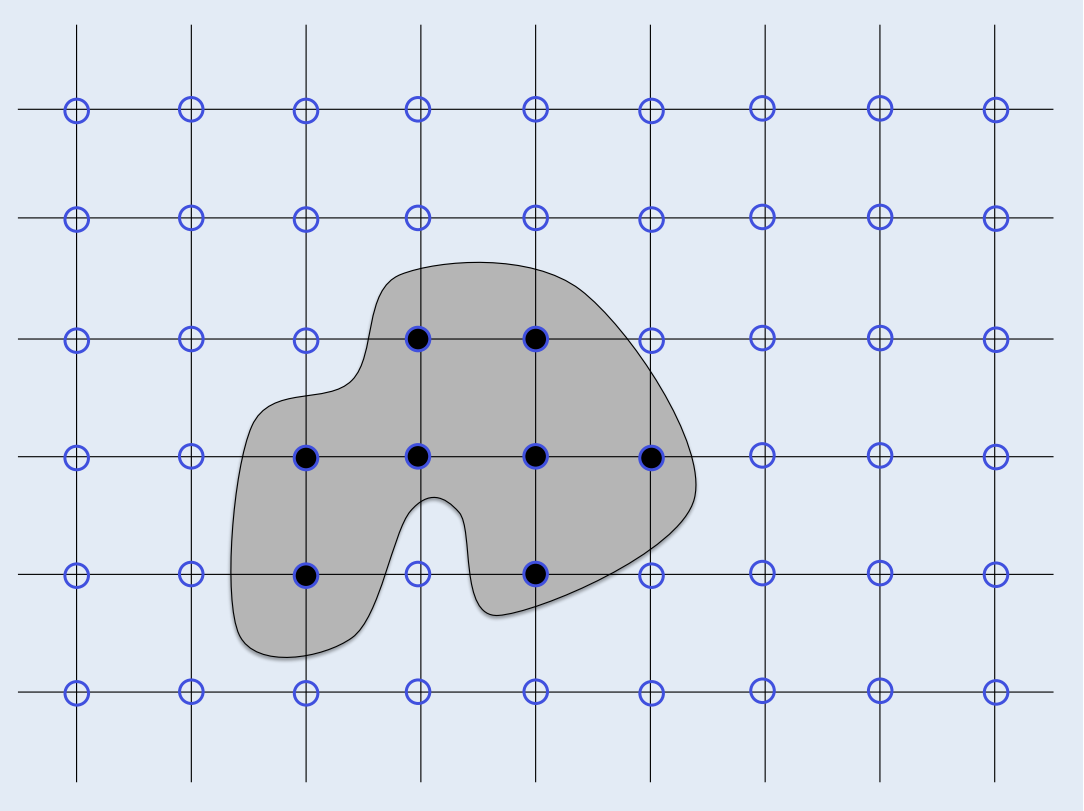

Figure 2.4: Representation of LBM domain that is to be treated by coupling method before being transferred to the solid solver.

To overcome the difference in boundary representation, the LBM fluid field is first promoted to a continuous representation that the meshfree method with distance fields can readily access. Until this conversion, it is almost certain that the the position in the fluid field that the meshfree method with distance fields queries will not contain any field information. Referencing Figure 2.4, it is seen that the boundary of the MMDF representation does not intersect a single LBM node where the fluid field data is obtained. As such, it is not possible to pass the pressure field from LBM to the MMDF as a boundary condition. This is ultimately overcome by employing bilinear interpolation at the boundary point using the field data at the four corners of the "cell". This idea is illustrated in Figure 2.5 where the yellow circle represents the intermediate interpolation before the second and final interpolation yielding the fluid field information at the desired

location designated by a green circle.

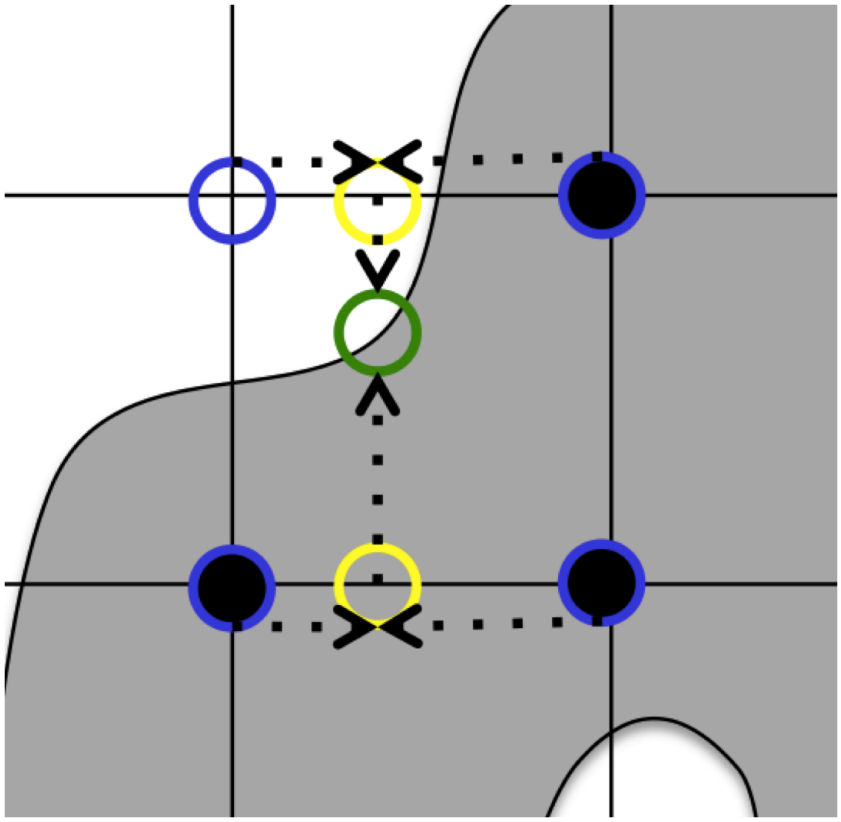

Figure 2.5: Boundary values used in the meshfree method with distance fields are extracted from the LBM fluid field via bilinear interpolation.

Notice that in Figure 2.5 that the bilinear interpolation occurs over a cell comprised of three solid nodes with no information from the LBM-generated pressure field. These "empty" nodes will reduce the accuracy of the final interpolated value on the boundary of the continuous MMDF domain representation. To remedy this, the fluid field is first "healed" through global interpolation, filling in the "empty" nodes with finite values that will then allow for successful bilinear interpolation. The key to the interpolation is that the entire field is interpolated utilizing only the nodes designated as fluid nodes and ignoring the solid nodes. This results in the empty solid nodes taking a value intermediate of the first fluid nodes outside of the boundary in the direction of interpolation.

The first stage of the global interpolation is to interpolate each row considering only the nodes designated as fluid (Figure 2.6). In this research, the interpolation is done

using a cubic spline, but the choice of interpolation scheme at this point is variable. Once the interpolation of the row is completed, the solid nodes are updated with new values from the interpolation. This occurs for each row in the domain. Once the row by row interpolation and solid node update is completed, the same procedure is conducted for every column (Figure 2.7). The field data collected from the row by row analysis and the column by column analysis is then averaged at each solid node, providing the final interpolation value for the previously empty solid nodes. They are now suitable for the previously described bilinear interpolation. The MMDF will be able to pull a parameter from anywhere within the domain, meaning exactly at the boundary where it will be exactly satisfied by the MMDF.

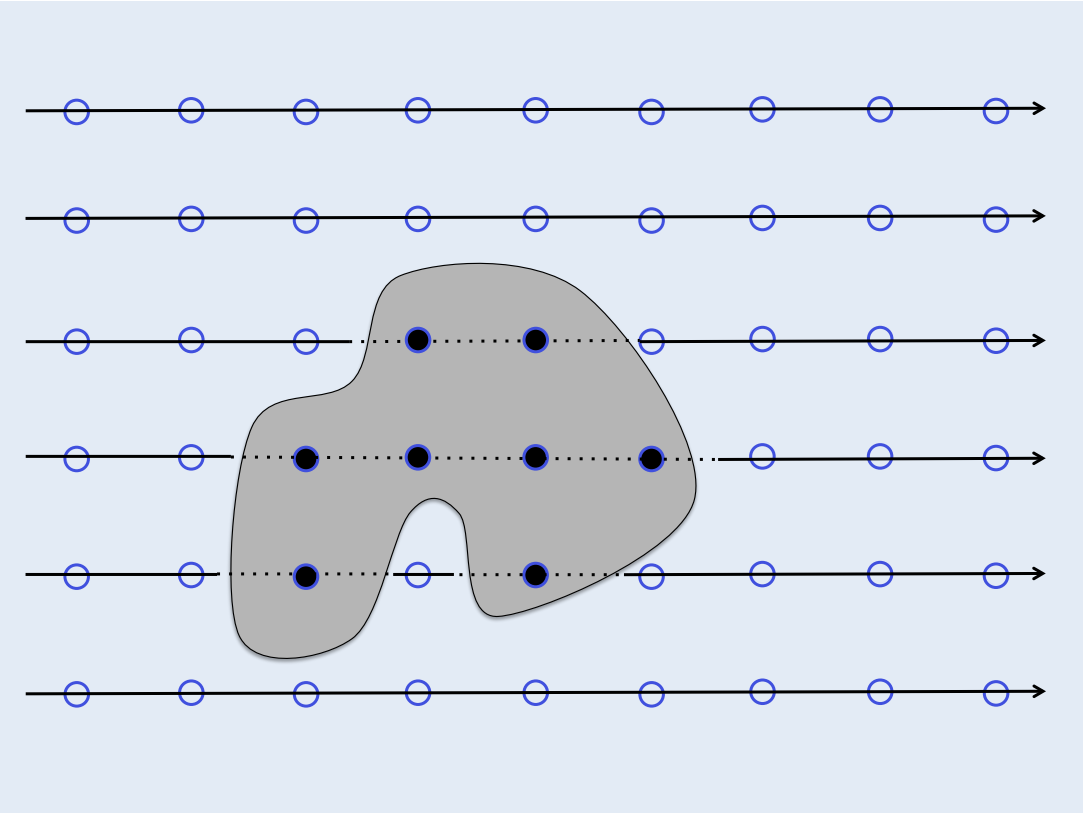

Figure 2.6: Each row is first interpolated individually, only including fluid nodes. Solid nodes are then populated from the interpolation value at their location.

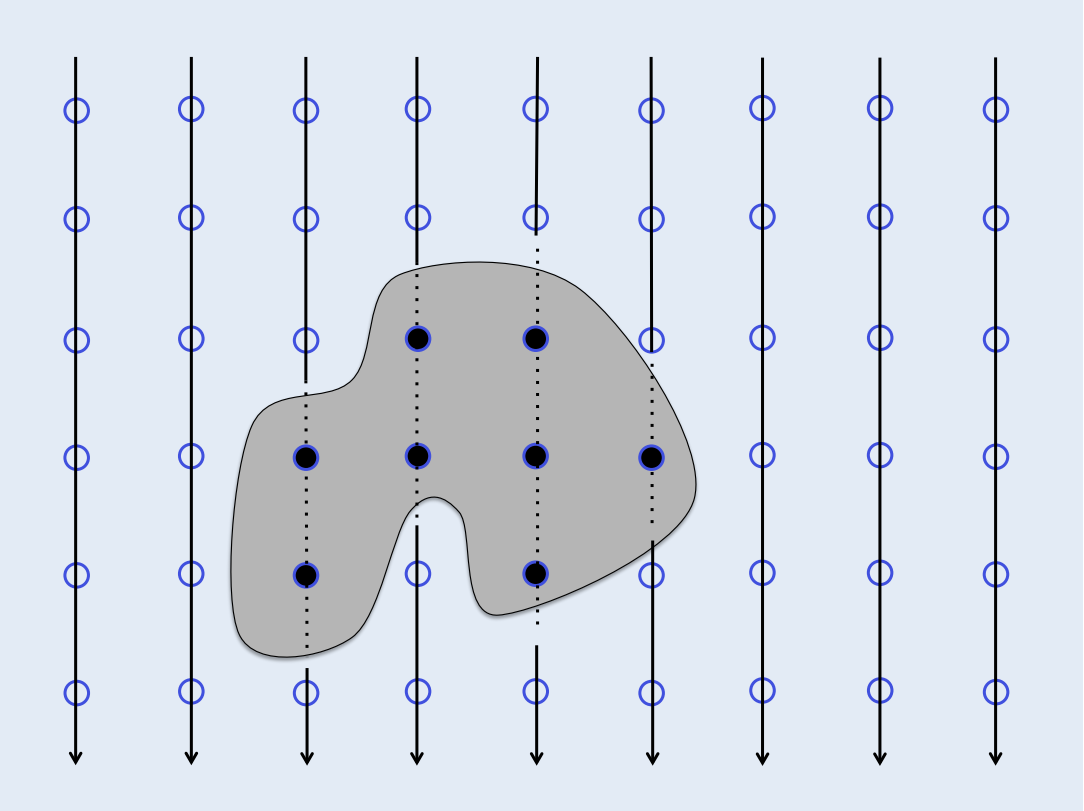

Figure 2.7: Each column is interpolated individually, only including fluid nodes. Solid nodes are then populated from the average of the column-interpolation value and row-interpolation value at the solid node location.

CHAPTER 3

NUMERICAL EXPERIMENTS

3.1 FSI Model Verification

Before applying the developed model, it was first verified via an analytically solvable, hydrostatic problem. The problem was designed to demonstrate three functionalities. Firstly, the fluidic component of the analytical problem was used to demonstrate that the LBM would provide the expected fluid field under given conditions. Secondly, the structural component of the verification was designed to ensure that the meshfree method with distance fields would predict the analytical solution for stress and deformation provided the hydrodynamic loading. Finally, the coupling method is verified by transferring the load from the pressure field, which is provided by LBM, to the meshfree method with distance fields as a boundary condition.

3.1.1 Lattice Boltzmann Method Verification

Figure 3.1 provides the fluidic problem description. It can be described as an infinite tank filled with water under Earth's gravitational pull and zero pressure at the surface of the fluid. The problem is then represented in dimensionless values used for the lattice Boltzmann simulation in Figure 3.2. In the lattice Boltzmann method simulation, the gray walls are populated with inactive solid nodes while the blue region is initialized with fluid nodes. Equation (3.1) defines the expected solution field, where P represents pressure, ρ represents density, g represents gravitational acceleration and h represents depth from the surface. With gravity and density remaining constant, pressure is expected to increase linearly with depth. Complete calculations for the LBM component of the verification can be found in the appendix, section 5.

The results for the LBM simulation of the hydrostatic condition for verification are presented quantitatively in Table 3.1 and visually in Figure 3.3. It can be seen in the table that the numerically determined maximum pressure found at the bottom of the tank agrees with the analytically determined value with an acceptable relative error of less than 1%. Figure 3.3 shows a linearly increasing pressure starting from the top (surface) of the fluid body all the way to the bottom, as predicted by Equation (3.1).

$$P = \rho g h \tag{3.1}$$

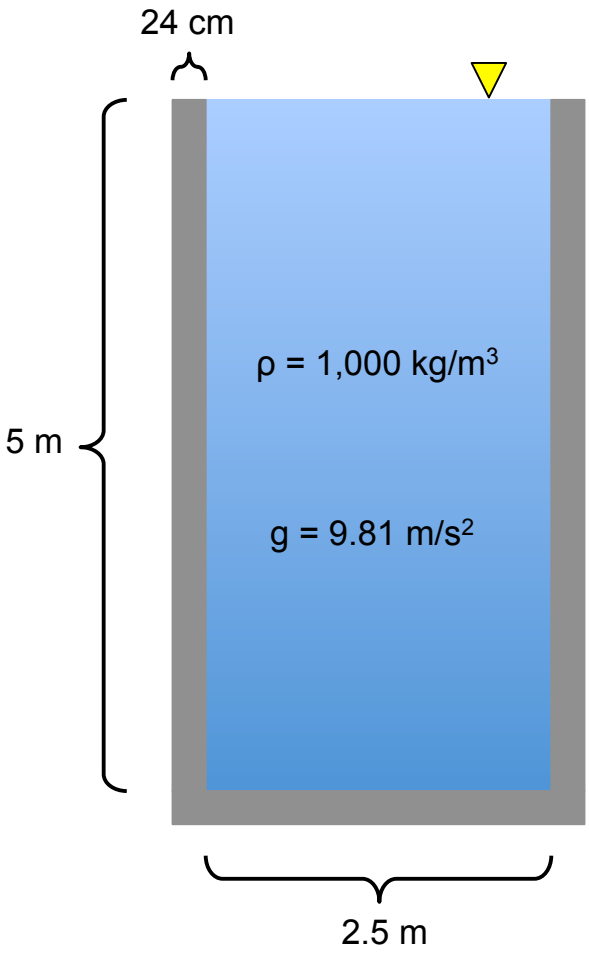

Figure 3.1: Fluidic problem description using physical units.

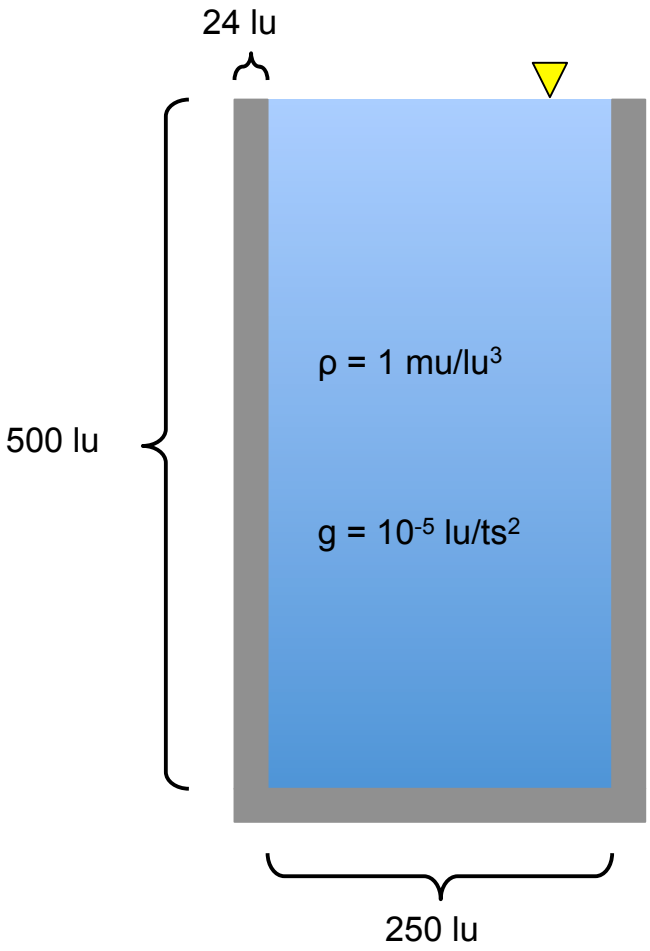

Figure 3.2: Fluidic problem description using non-dimensional lattice units.

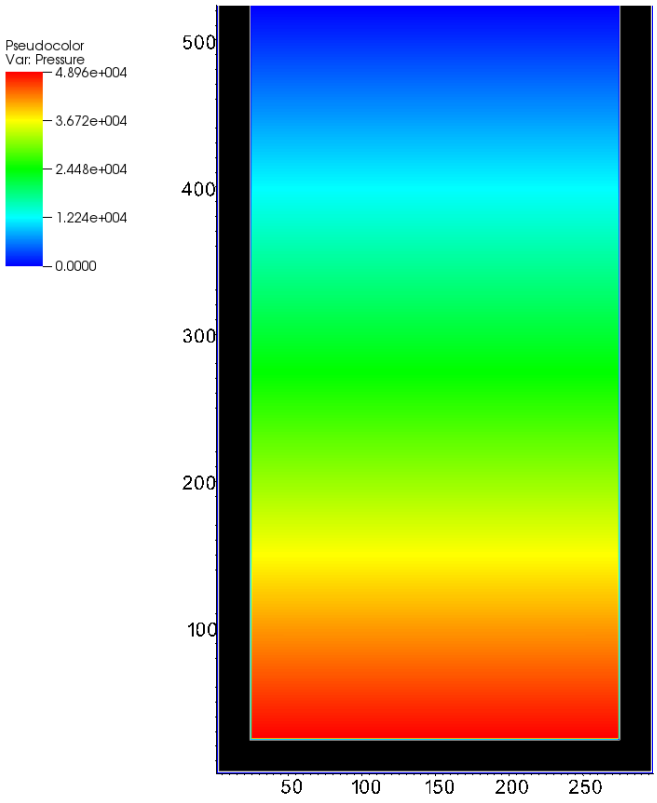

Figure 3.3: Pressure field from fluid component of verification. Legend units are in Pascals. Black border represents solid, inactive portion of domain.

Analytical Max (Pa)	Numerical Max (Pa)	Relative Error (%)
49050	48960	0.18

Table 3.1: Comparison between analytically and numerically determined maximum pressures.

3.1.2 Coupling Method and Meshfree Method Verification

Once the LBM verification was completed, it was necessary to then verify that the resulting fluid field data was accurately being passed to the meshfree method with distance fields and that the meshfree method with distance fields utilizes the data to provide accurate structural results. To conduct this verification, the pressure field from the hydrostatic solution illustrated in section 3.1.1 was applied to the gray structure

shown in Figure 3.1. The simple geometry and loading condition allows for analytical calculation and prediction of the maximum displacement that occurs at the free end of the cantilevered beam. These calculations have been included in the appendix in section 5. In addition to analytical determination of the maximum deformation, it was also determined via finite element analysis using the SolidWorks CAD software.

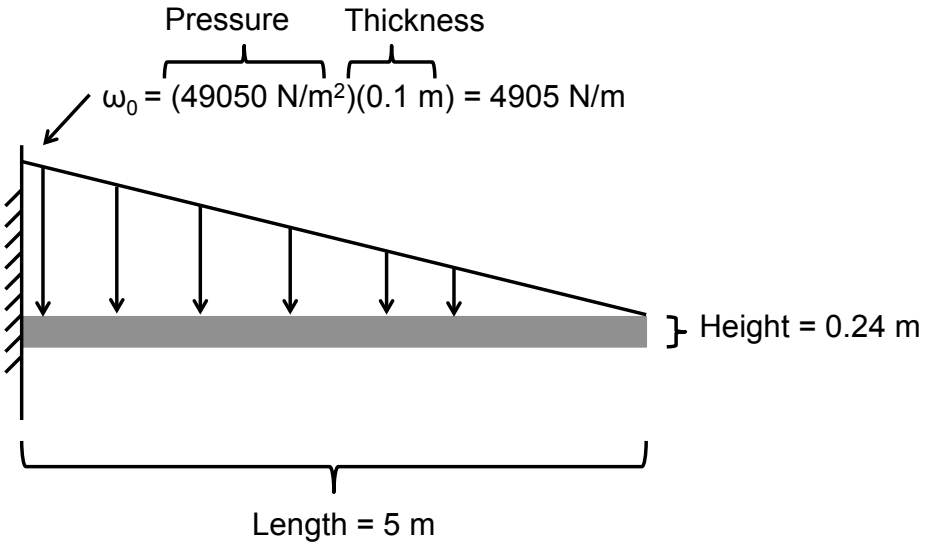

Figure 3.4: Analytical model for structural problem for meshfree method with distance fields verification.

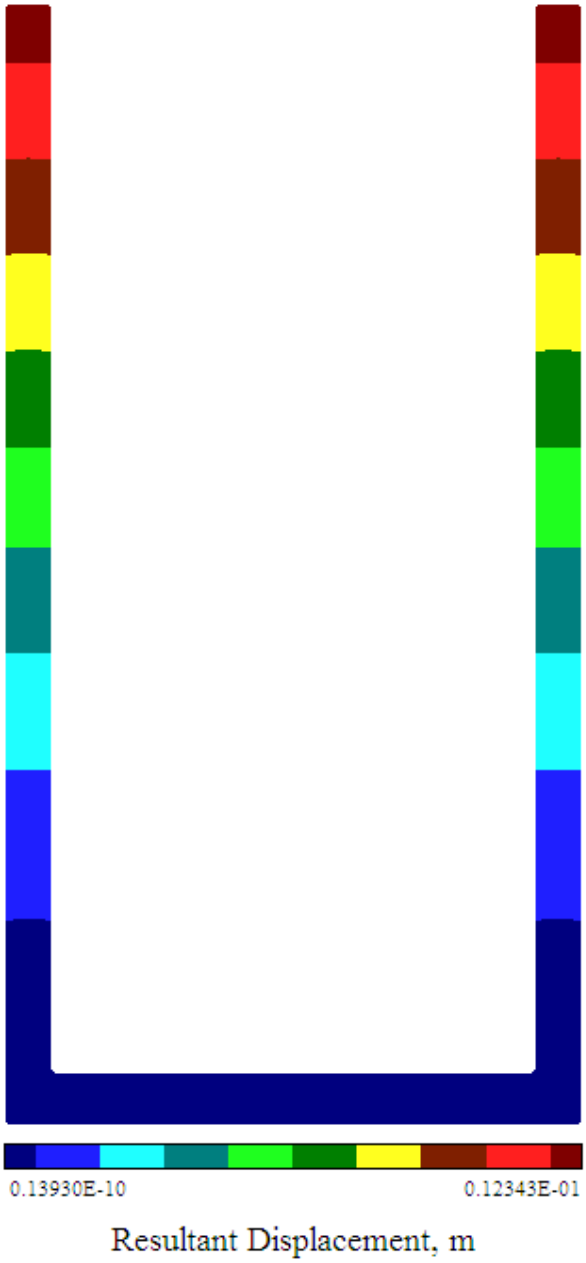

Figure 3.5: Displacement results from meshfree method with distance fields using LBM-generated pressure field and passed using the coupling method described in section 2.3.

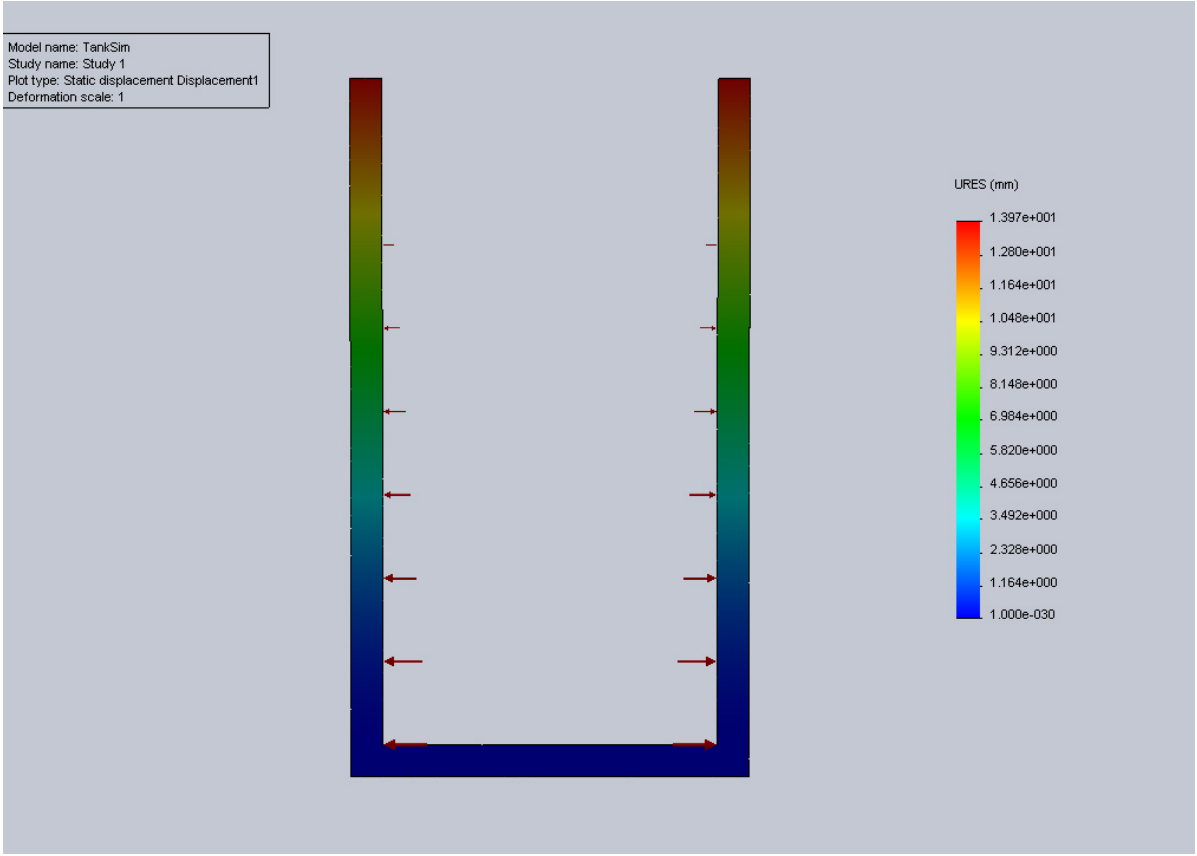

Figure 3.6: Displacement results from Solidworks Simulation, applying a linear increasing pressure boundary condition representing the hydrostatic fluid pressure load.

	Result (mm)	Relative Error (%)
Analytical	12.85	-
SolidWorks	13.97	8.72
Developed Method	12.34	3.97

Table 3.2: Maximum displacement results from structural and coupling model verification experiments.

The results for this test are presented in Table 3.2. It can be seen that the results from the proposed coupling model and structural analysis method agree with the analytical solution to within engineering accuracy. Additionally, it is noticed that the results from the proposed method fall between the analytical solution and the numerical solution provided by SolidWorks.

3.2 Convergence of the Interpolation Algorithm at Solid-Fluid Interface

An important criteria used to measure the quality of a numerical method is convergence. As the number of elements and nodes are increased, the approximate values should approach the exact values. For the coupling method proposed in this research, the numerical method of interest is the set of interpolation schemes used to extrapolate the field data from the discrete geometric boundary representation of LBM to the continuous boundary utilized by the meshfree method with distance fields. As the quantity of interpolation points used to represent the LBM solution field is increased (mesh resolution), the interpolated values at the continuous meshfree method boundary should monotonically approach the exact values.

To investigate the convergence properties of the coupling method, an experiment was conducted using simple geometries. Figure 3.7 illustrates the geometries employed for the convergence study. A circle (3.7(a)) was selected to provide the simplest case of a continuous, axisymmetric geometry. The second geometry is a cross shape (3.7(b)) that introduces sharp ninety degree angles to the interpolation scheme. Instead of experimenting with a solution field generated by an LBM simulation, several two-dimensional analytical functions were used to evaluate the interpolation scheme. Equations (3.2), (3.3) and (3.4) were used as test functions for analyzing the convergence of the interpolation scheme. Figure 3.8 illustrates the test fields described by the aforementioned equations.

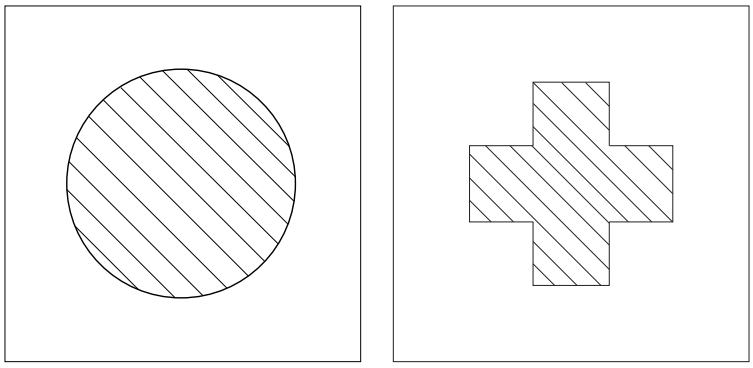

(a) Simple circular geometry. (b) Cross geometry with sharp angles.

Figure 3.7: Problem setup for convergence experiments. Hatched area represents solid geometry where data is excluded from interpolation. White space is defined by functions and included in interpolation.

$$f_1(x, y) = 1 + 2x + 3y + 4xy + 5x^2 + 6y^2 \tag{3.2}$$

$$f_2(x, y) = y^2 - x^2 \tag{3.3}$$

$$f_3(x, y) = sin(x) + cos(y) \tag{3.4}$$

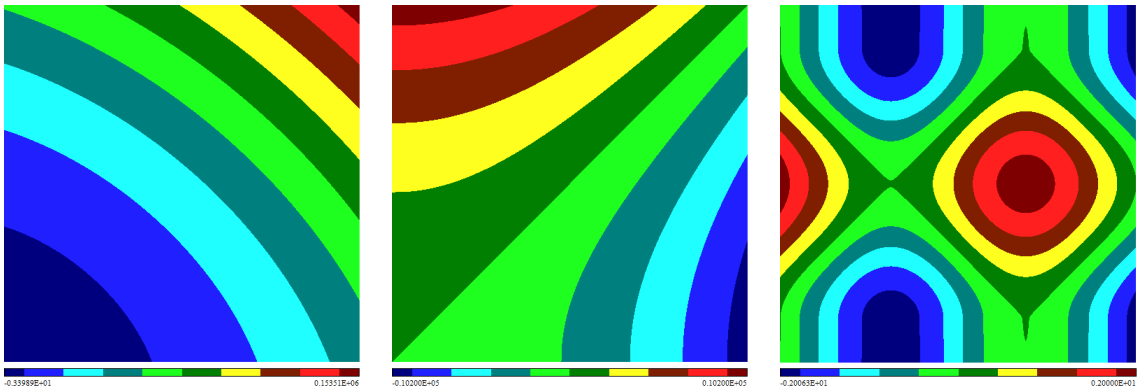

(a) Equation (3.2) (b) Equation (3.3) (c) Equation (3.4)

Figure 3.8: Analytical functions used to demonstrate interpolation convergence.

To study convergence, the quantity of nodes used to interpolate the analytical function were varied, keeping them uniformly spaced. The quantity of nodes used were

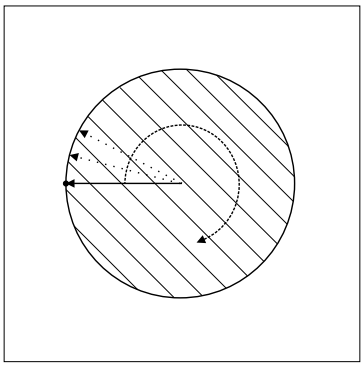

Figure 3.9: Test points are evaluated at the boundary of the test geometry in one degree increments beginning at the left-most point.

powers of ten beginning with one hundred and ending with one million. The parameter used to measure convergence was the maximum relative error from three hundred sixty points collected around the boundary of the test geometries. These points were determined by rotating a ray from the center of the geometry towards its boundary in one degree increments, clockwise, starting from zero degrees positioned at left. This procedure is illustrated by Figure 3.9.

At the intersection of the ray and the boundary, the interpolated value was extracted and the analytical value was evaluated. Finally the maximum relative error was calculated. Figure 3.10, Figure 3.11 and Figure 3.12 illustrate the closure of the gap between the profiles of the interpolated boundary values and the analytical boundary values. It can be seen in each of these three figures that the error definitively converges to zero with increasing quantity of interpolation points. Additional figures are included in the appendix in section 5. Table 3.3 summarizes the convergence study for all six cases.

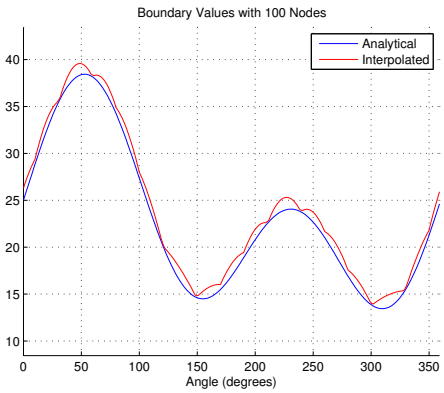

(a) 100 nodes.

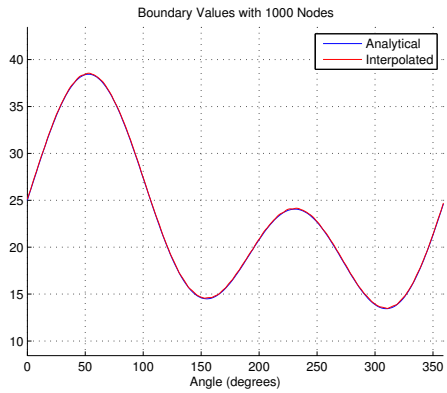

(b) 1,000 nodes.

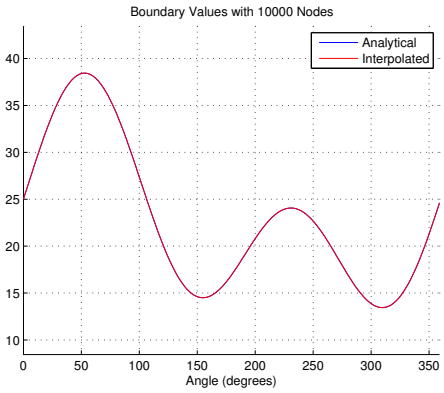

(c) 10,000 nodes.

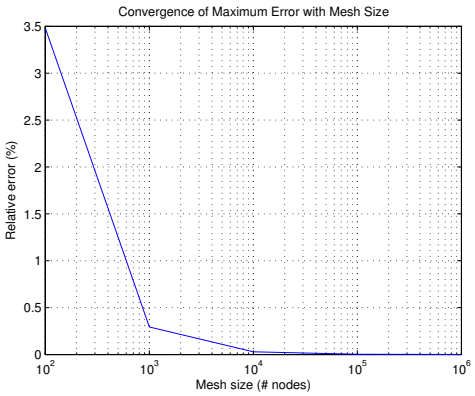

(d) Convergence of maximum relative error.

Figure 3.10: Convergence of Equation (3.2) on boundary of circle geometry.

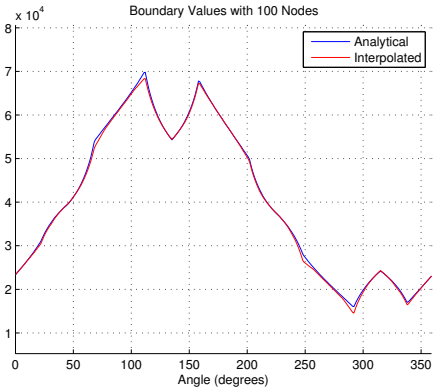

(a) 100 nodes.

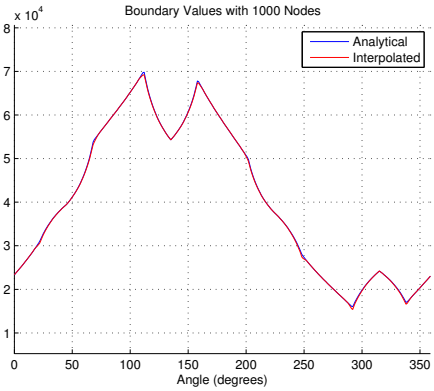

(b) 1,000 nodes.

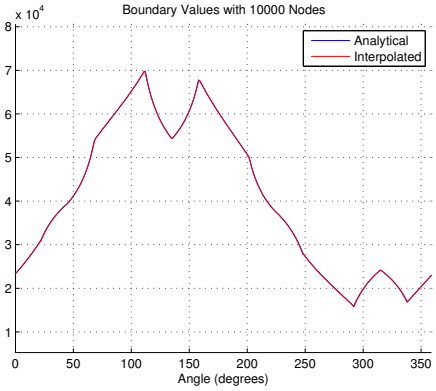

(c) 10,000 nodes.

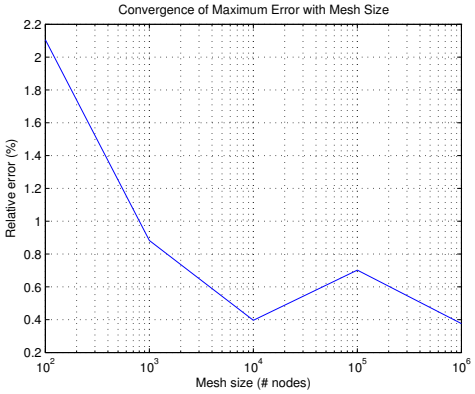

(d) Convergence of maximum relative error.

Figure 3.11: Convergence of Equation (3.2) on boundary of cross geometry.

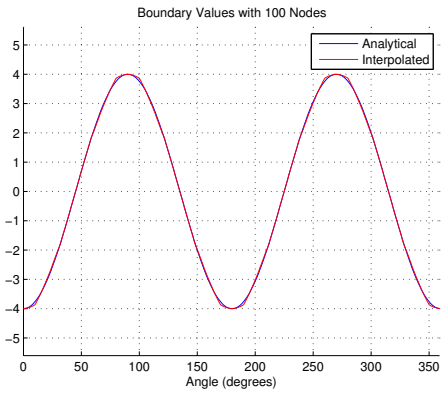

(a) 100 nodes.

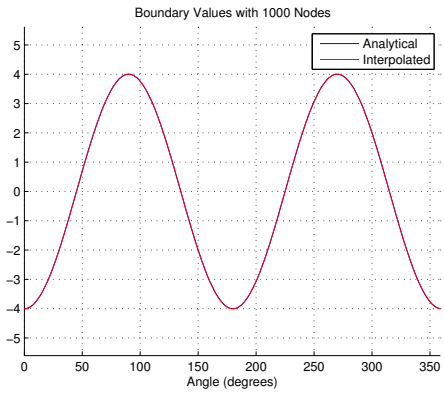

(b) 1,000 nodes.

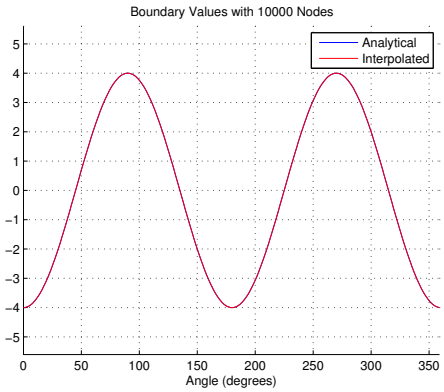

(c) 10,000 nodes.

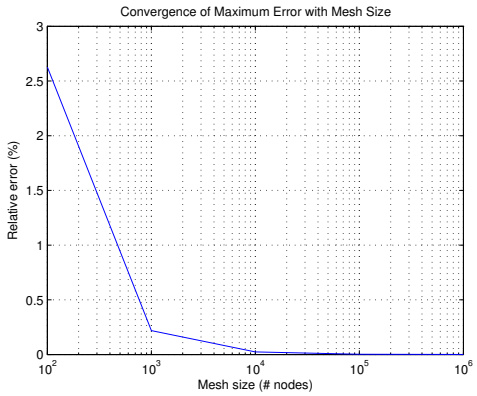

(d) Convergence of maximum relative error.

Figure 3.12: Convergence of Equation (3.3) on boundary of circle geometry.

Table 3.3: Maximum Relative Error in Convergence Study (%)

	Circle			Cross		
# Nodes	$f_1(x,y)$	$f_2(x,y)$	$f_3(x,y)$	$f_1(x,y)$	$f_2(x,y)$	$f_3(x,y)$
10^2	3.4776	2.6262	9.7606	2.1055	6.8785	3.5585
10^3	0.2937	0.2182	0.9071	0.8827	2.5683	2.1651
10^4	0.0286	0.0241	0.0943	0.3961	1.1559	1.1826
10^5	0.0029	0.0025	0.0094	0.7022	2.0461	1.7205
10^6	0.0005	0.0003	0.0010	0.3762	1.0958	1.1224

3.3 Demonstration Case 1: Flow through a restricted channel

Upon completion of verification of the FSI model against the analytical hydrostatic fluid problem and distributed cantilever beam problem, several demonstration cases were created to qualitatively exhibit the performance of this FSI method. The first case under

study is a simple simulation of channel flow with single wall obstruction. The flow is driven by a body force (gravity) with no-slip wall boundaries on the top and bottom of the channel. The left and right sides of the channel are prescribed as periodic boundarys whereby the flow exiting the right will re-enter on the left. Under this flow condition, the wall behaves as a cantilevered beam with the flow around it forcing deflection. It should be noted that all results for the demonstration simulations are fictictious and only intended to show the relationship between the flow field and resulting deformation in the solid. Figure 3.13 illustrates the described case of channel flow, with a wall diverting the flow. In Figure 3.13 you can see that the fluid entering the channel can be approximated as uniformly distributed with typical Poiseuille behavior. After entering the channel, the fluid is forced through the gap between the obstructive wall and the top of the channel, accelerating the fluid all the while, as made visible by the red region in the figure. After the wall, the fluid recovers its Poiseuille profile.

Figure 3.14 illustrates the pressure field in the channel flow that accompanies the velocity field depicted in Figure 3.13. It can be seen that there is a high pressure immediately in front of the wall obstruction in the channel. When compared with the velocity field, it is understood that the pressure field is generated as a result of the severe deceleration of the fluid being blocked by the wall. The downstream behavior of the pressure field is approximately uniform. The pressure gradient across the wall is expected to result in the wall deforming in the downstream direction. Figure 3.15 illustrates the results from the structural analysis of the wall based on the use of the fluid pressure field as a boundary condition. As expected, the wall deforms in the downstream direction in true cantilever fashion with the largest deformation at the tip of the wall.

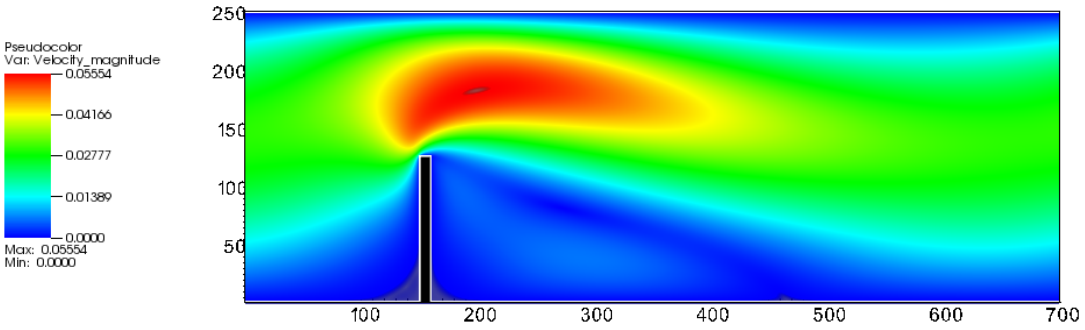

Figure 3.13: The resulting velocity field from a body-force driven fluid flow through an impeded channel.

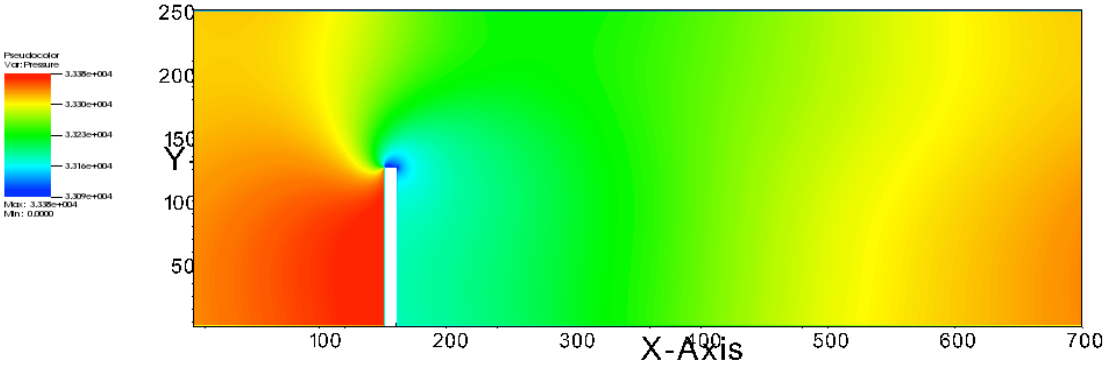

Figure 3.14: The resulting pressure field from a body-force driven fluid flow through an impeded channel.

Figure 3.15: The resulting solid stress distribution from a body-force driven fluid flow through an impeded channel.

3.4 Demonstration Case 2: Flow past an irregular body.

The second test case follows the first in simulating channel flow. Instead of a solid wall protruding from the wall of the channel, an irregularly shaped body is centered in the fluid field. The intent for this test case is to show an ambiguous body with sharp corners (mesh-resistant) directing the fluid flow and deflecting at the same time. Figure 3.16 is a depiction of the body. The edges with arrows indicate boundaries that are to extract a normal load from the LBM-generated pressure field. The circle in the center of the body is used to fix the body in two dimensions. A zero displacement boundary condition is applied along the perimeter of the circle. After the object was sketched, it was immersed into the same channel conditions as described in the demonstration case described in section 3.3. The resulting velocity field is presented in Figure 3.17. Instead of the high velocity region being off to one side due to the protruding wall, the high velocity regions are spread symmetrically to either side of the channel. Figure 3.18 illustrates the pressure field about the irregular body after the flow has reached steady-state. As in the case of the restricted channel in section 3.3, there is a high-pressure region directly in front of the body, where the fluid decelerates.Once obtained, the pressure field is passed through the coupler to the solid structure solver resulting in the stress distribution seen in Figure 3.20. It is observed that the stress in the obstruction is heavily concentrated at the circle fixture and minimal through the rest of the body. This stress results in the displacement that is presented in Figure 3.19. The displacements seen here are sensible in that the smallest displacements are near the fixed boundary and increase towards the extremeties of the body where there are thinner members and less influence from the fixed boundary.

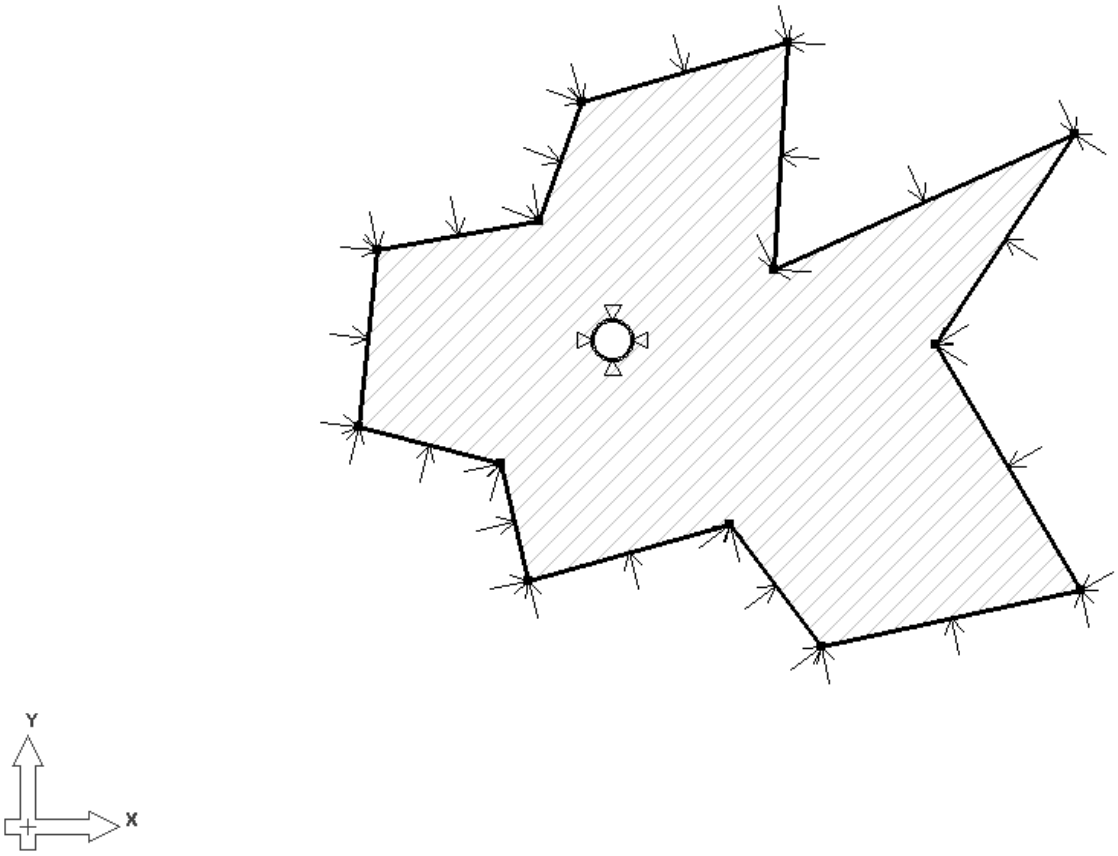

Figure 3.16: This is a sketch of a semi-complex boundary with sharp corners. It is immersed in channel flow for this study.

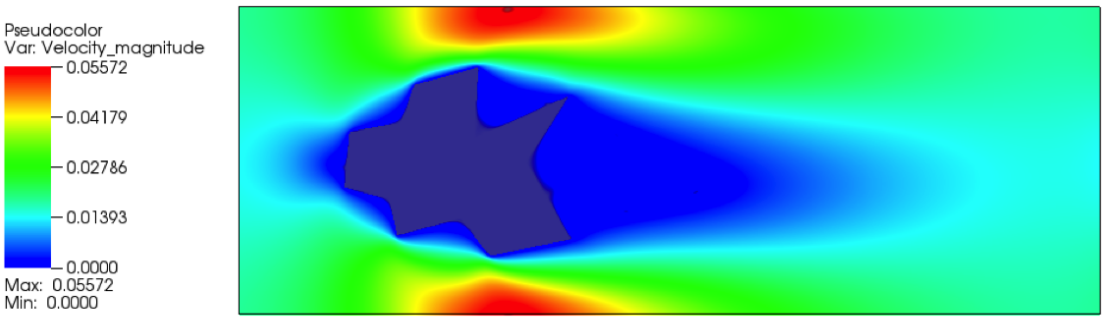

Figure 3.17: Resulting velocity field from channel flow around irregularly shaped geometry displayed in Figure 3.16.

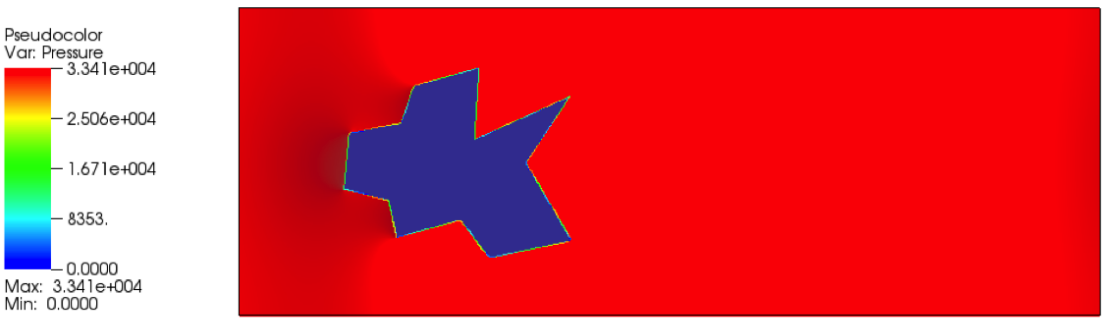

Figure 3.18: Resulting pressure field from channel flow around irregularly shaped geometry displayed in Figure 3.16.

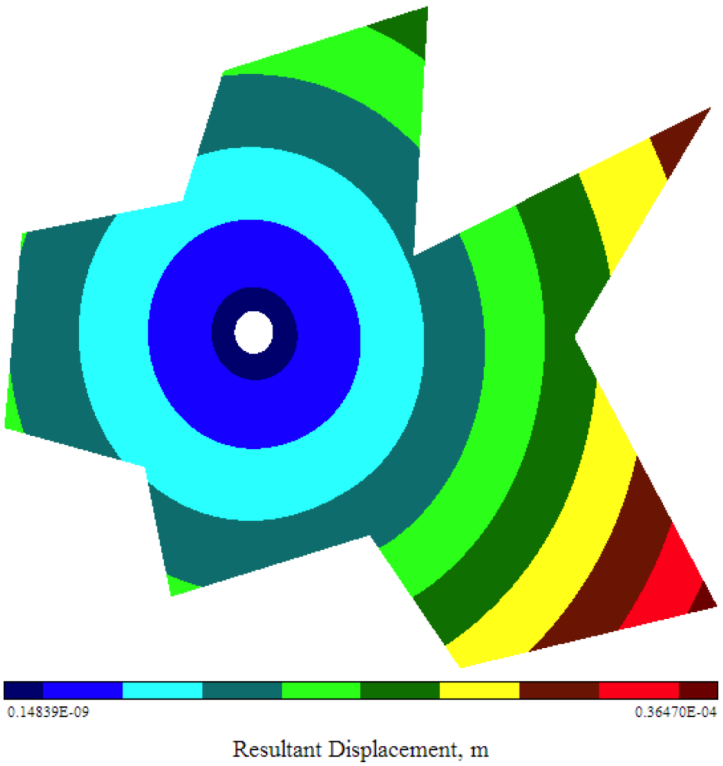

Figure 3.19: Resulting displacement of irregular body from channel flow.

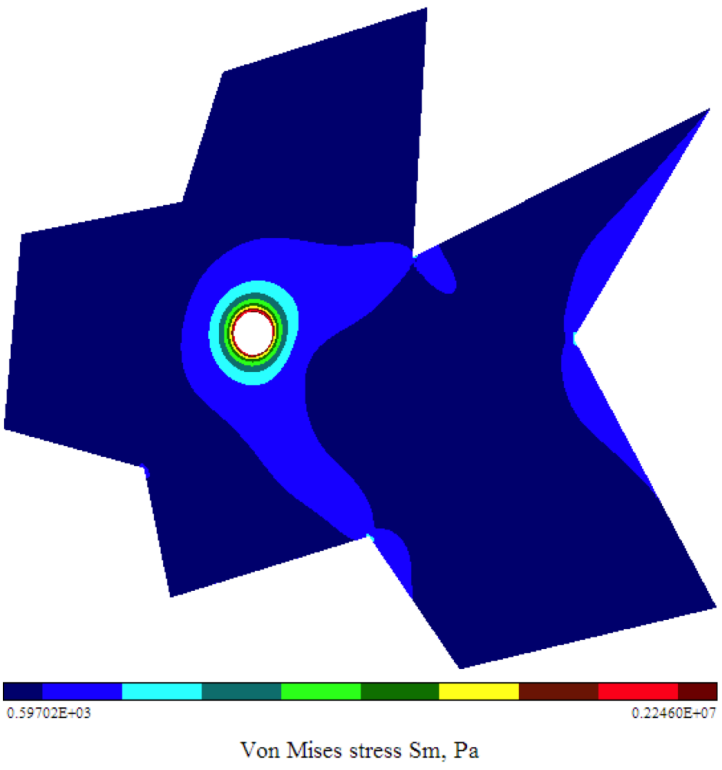

Figure 3.20: Resulting stress within irregular body from channel flow.

CHAPTER 4

DISCUSSION AND CONCLUSION

In this research, the feasibility of coupling of the lattice Boltzmann method and the meshfree method with distance fields as a fluid-structure interaction model has been demonstrated. The lattice Boltzmann method was verified by utilizing a hydrostatic pressure distribution in a two-dimensional tank. The pressure distribution generated by the lattice Boltzmann method was used to verify the developed coupling method as well as the meshfree method with distance fields. Upon verification, the coupling method convergence was studied by interpolating over three separate functions and with each function over multiple domains. Convergence was observed and observed to be monotonic for the test cases presented here. Two demonstrations of the FSI model working in concert were presented. One demonstration was of channel flow impeded by a wall stemming from the channel wall. The second demonstration was of an irregular body fixed in the center of a channel. A qualitative analysis was conducted on both and all results are as expected.

The method presented here for communicating pressure field data from the lattice Boltzmann method to the meshfree method with distance fields is expandable to other field data that can be provided by the lattice Boltzmann method. For example, the lattice Boltzmann method is capable of simulating convective heat transfer through a fluid field. It is possible to transfer temperature field data from the LBM to the MMDF at the boundary and determine the conduction behavior through the solid body. Another example is mass transport. The LBM has also been shown to be capable of simulating solute transport. In this case, the parameter that would be transferred is concentration with the end result being simulation of particle diffusion into the solid as in the material case hardening process.

Although not demonstrated here, it is possible to provide feedback from the MMDF to the LBM by deforming the boundary in the LBM based on the results obtained by the MMDF. Methodologies for adjusting the solid-fluid interface with LBM have been demonstrated [18] and can be incorporated into this coupling model without issue. This will allow for typical oscillatory behaviors to be simulated as well as a more

intimate interaction between the solid and fluid. It is recommended in future work that a batch program be written to automatically run the pair of solvers and the coupler, updating the domain as it goes.

The coupling model presented in this thesis is readily extendable to three dimensions. Any interpolation scheme can be used for global interpolation. Local interpolation can be done using bi-quadratic interpolation and so forth. The method can be applied to a nonuniform mesh as well. In parallel computing, global interpolation would require full domain information, but bilinear interpolation can be conducted within the subdomain. It may be possible to restrict the global interpolation to a subdomain with further investigation. It may be interesting to also configure a completely parallel FSI solver based on the ideas presented here.

In future work, it is very desirable to integrate more organic, complex domains in FSI simulation to further demonstrate the capacities of this research. The work presented in this thesis was constrained to CAD generated geometries. The complex geometry handling has been demonstrated for the meshfree method with distance fields alone [1] and using the lattice Boltzmann method alone [8]. The next step would be to pose this sort of challenge to the coupled model. For example, a geometric scan of piece of coral could be imported into the FSI simulation tool with varying fluid flow to study stress distributions in the coral.

CHAPTER 5

APPENDICES

LBM Verification via Hydrostatic Condition

In order to simulate the problem described in section 3.1, it was first necessary to translate the parameters from physical space to non-dimensional "lattice space". Equation (5.1) is used to ensure similitude. This equation is used to derive equation (5.2) which defines the relationship between the solved value, lattice pressure, and the desired value, physical pressure.

$$\frac{P}{\rho g h} = \frac{P_{LBM}}{\rho_{LBM} g_{LBM} h_{LBM}} \tag{5.1}$$

$$P = P_{LBM} \frac{\rho g h}{\rho_{LBM} g_{LBM} h_{LBM}} \tag{5.2}$$

$$g_{LBM} = 0.00001 \ \frac{lu}{ts^2} \tag{5.3}$$

$$h_{LBM} = 500 \ lu \tag{5.4}$$

$$\rho_{LBM} = 1 \ \frac{mu}{lu^3} \tag{5.5}$$

$$g = 981 \ \frac{cm}{s^2} \tag{5.6}$$

$$h = 500 \ cm \tag{5.7}$$

$$\rho = 1000 \ \frac{kg}{m^3} = 0.001 \ \frac{kg}{cm^3} \tag{5.8}$$

Substituting Equations (5.3), (5.4), (5.5), (5.6), (5.7), (5.8) into (5.2) yields...

$$P = P_{LBM}\frac{(0.001\ \frac{kg}{cm^3})(981\ \frac{cm}{s^2})(500\ cm)}{(1\ \frac{mu}{lu^3})(0.00001\ \frac{lu}{ts^2})(500\ lu)} = P_{LBM}\frac{490.5\ \frac{kg\ cm}{s^2\ cm^2}}{0.005\ \frac{mu\ lu}{ts^2\ lu^2}} \tag{5.9}$$

The right hand side of equation (5.9) is then multiplied by a conversion factor to output the physical pressure in Pascals...

$$P = P_{LBM}\frac{490.5\ \frac{kg\ cm}{s^2\ cm^2}\ \frac{100\ cm}{m}}{0.005\ \frac{mu\ lu}{ts^2\ lu^2}} = P_{LBM}9810000\frac{\frac{kg\ m}{s^2\ m^2}}{\frac{mu\ lu}{ts^2\ lu^2}} \tag{5.10}$$

The expected physical pressure is calculated using equation (3.1)...

$$P = (9.81\frac{m}{s^2})(5\ m)(1000\frac{kg}{m^3}) = 40950Pa \tag{5.11}$$

Analytical Calculations for the Verification of the Coupling Method and Meshfree Method with Distance Fields

The problem selected for verification allows for analytical prediction of the maximum displacement of the gray structure in Figure 3.1. The analysis of the structure can be approximated as a cantilevered beam with a linearly varying distributed load as depicted in Figure 3.4. For this loading condition, Equation (5.12) can be used to describe the maximum displacement, δ_{max}, which occurs at the free end of the cantilevered beam. In Equation (5.12), ω_0 represents the maximum load, I represents the cross-sectional moment of inertia, l represents the length of the beam, and E represents the elastic modulus of the material. Allowing the material to be Aluminum 1060, the elastic modulus, E, is 69 GPa. The length of the beam is described in Figure 3.4 and is equal to 5 meters.

$$\delta_{max} = \frac{\omega_0\ l^4}{30EI} \tag{5.12}$$

$$I = \frac{1}{12}bh^3 = \frac{1}{12}(0.1\ m)(0.24\ m)^3 = 0.0001152\ m^4 \tag{5.13}$$

$$\delta_{max} = \frac{(4905\frac{N}{m})(5\ m)^4}{(30)(69\ GPa)(0.0001152\ m^4)} = 12.85\ mm \tag{5.14}$$

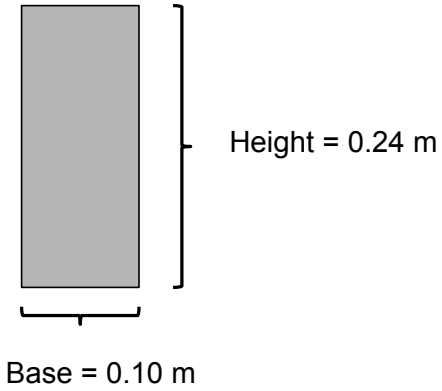

Figure 5.1: Cross-sectional dimensions of beam used in structural analysis.

Convergence Results

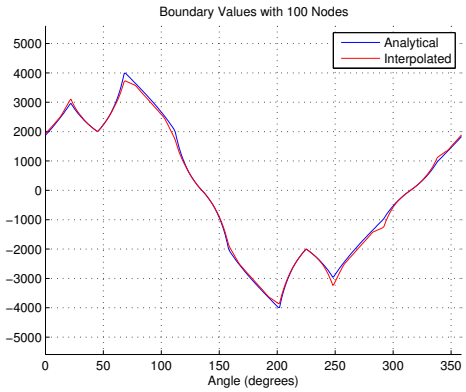

(a) 100 nodes.

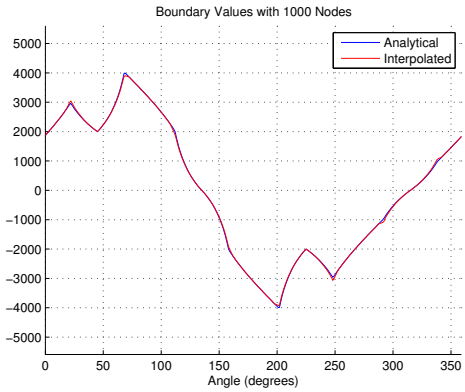

(b) 1,000 nodes.

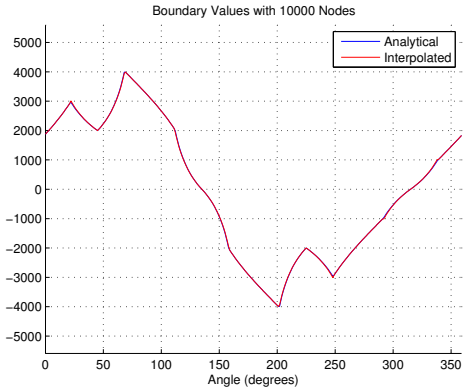

(c) 10,000 nodes.

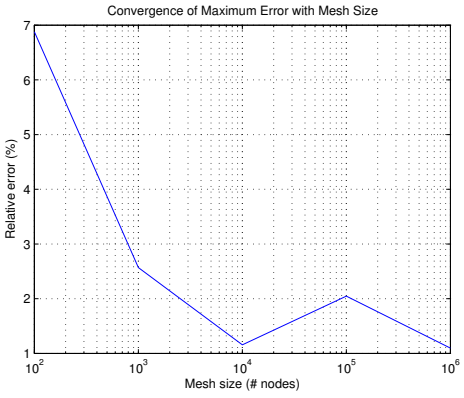

(d) Convergence of maximum relative error.

Figure 5.2: Convergence of Equation (3.3) on boundary of cross geometry.

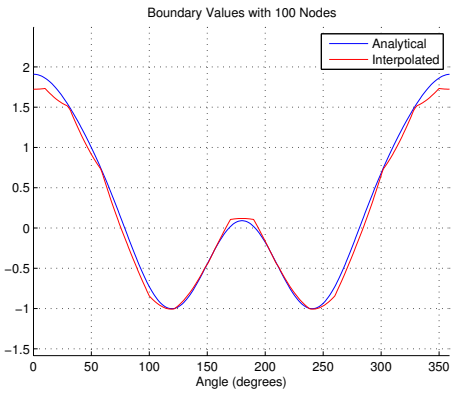

(a) 100 nodes.

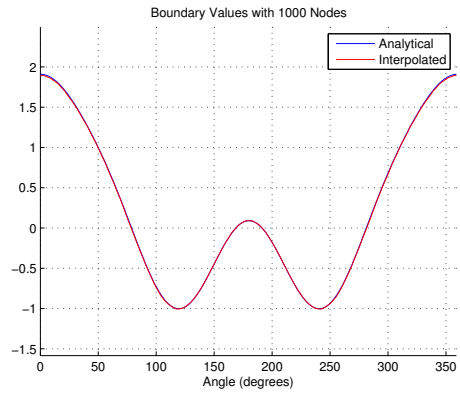

(b) 1,000 nodes.

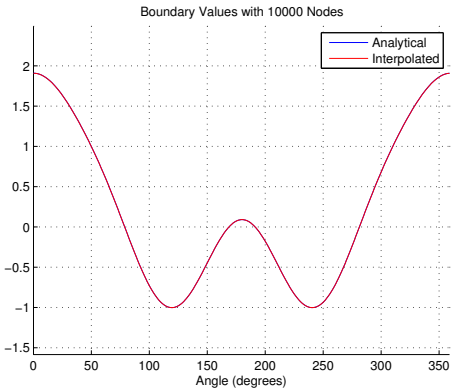

(c) 10,000 nodes.

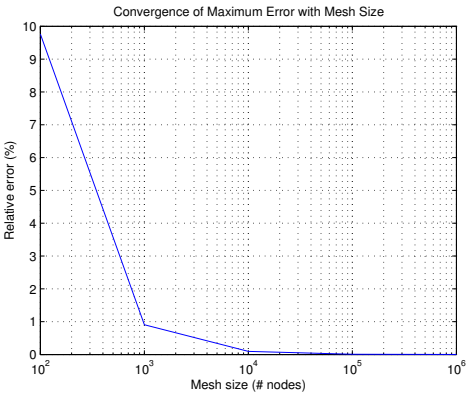

(d) Convergence of maximum relative error.

Figure 5.3: Convergence of Equation (3.4) on boundary of circle geometry.

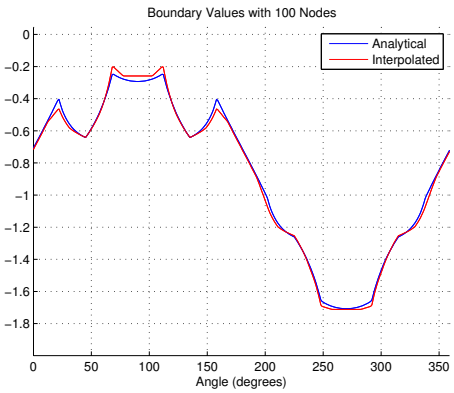

(a) 100 nodes.

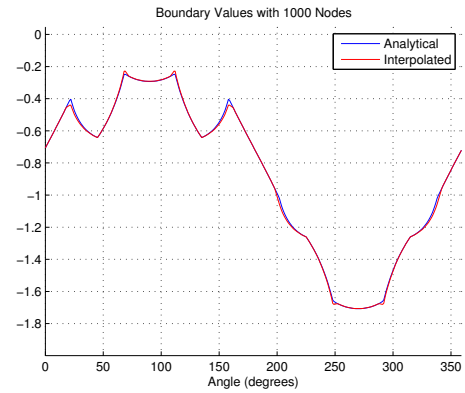

(b) 1,000 nodes.

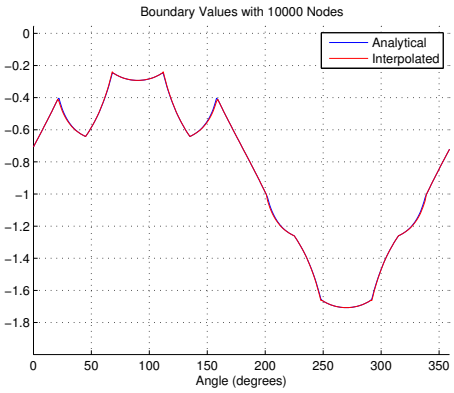

(c) 10,000 nodes.

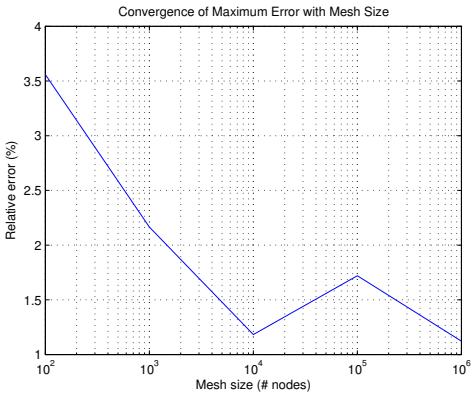

(d) Convergence of maximum relative error.

Figure 5.4: Convergence of Equation (3.4) on boundary of cross geometry.

REFERENCES

[1] M. Freytag, V. Shapiro, and I. Tsukanov. Finite elment analysis in situ. *Finite Elements in Analysis and Design*, 47(9):957–972, 2011.

[2] B. Clark. In *Proceedings of the 18th International Meshing Roundtable*, Verlag, 2009. Springer.

[3] S.A. Berger and L.D. Jou. Flows in stenotic vessels. *Annu. Rev. Fluid Mech.*, 32(347), 2000.

[4] V. Shapiro and I. Tsukanov. Meshfree simulation of deforming domains. *Computer-Aided Design*, 31(7):459–471, 1999.

[5] J. G. Zhou. *Lattice Boltzmann Methods for Shallow Water Flows*. Springer-Verlag, 2004.

[6] AJC Ladd. Short-time motion of colloidal particles: Numerical simulation via a fluctuating lattice-boltzmann equation. *Phys Rev Lett*, 70:1339–1342, 1993.

[7] X. Shan and H. Chen. Simulation of nonideal gases and liquid-gas phase transitions by the lattice boltzmann equation. *Phys Rev E*, 49:2941–2948, 1994.

[8] M.C. Sukop and D. Or. Lattice boltzmann method for homogeneous and heterogeneous cavitation. *Phys Rev E*, 71, 2005.

[9] S. Hou et al. A lattice boltzmann subgrid model for high reynolds number flows. *Fields Inst. comm.*, 6:151–166, 1996.

[10] J.A. Somers. Direct simulation of fluid flow with cellular automata and the lattice boltzmann equation. *Applied Sci. Res.*, 51:127–133, 1993.

[11] E. Aharonov and D.H. Rothman. Non-newtonian flow (through porous media):a lattice-boltzmann method. *Geophysical Research Letters*, 20:679–682, 1993.

[12] M.C. Sukop and D. Thorne. Lattice boltzmann model for the elder problem. In *Proceedings of XVth International Conference on Computational Methods in Water Resources*, Chapel Hill, NC, USA, 2004. Elsevier, Amsterdam.

[13] S. Piperno, C. Farhat, and B. Larrouturou. Partitioned procedures for the transient solution of coupled aeroelastic problems part i: Model problem, theory and two-dimensional application. *Computer methods in applied mechanics and engineering*, 124:79–112, 1995.

[14] C. Felippa, K.C. Park, and C. Farhat. Partitioned analysis of coupled mechanical systems. *Computer methods in applied mechanics and engineering*, 190:3247–3270, 2001.

[15] R. Mittal and G. Iaccarino. Immersed boundary methods. *Annu. Rev. Fluid Mechn.*, 37:239–261, 2005.

[16] C. S. Peskin. *Flow patterns around heart valves: a digital computer method for solving the equations of motion.* PhD thesis, Yeshiva University, 1972.

[17] X. Shi and S. P. Lim. A lbm-dlm/fd method for 3d fluid-structure interactions. *Journal of Computational Physics*, 226:2028–2043, 2007.

[18] S. Geller, S. Kollmannsberger, M. El Bettah, M. Krafczyk, D. Scholz, A. Duster, and E. Rank. An explicit model for three-dimensional fluid-structure interaction using lbm and p-fem. *Computational Science and Engineering*, 73, 2010.

[19] A. Joshi, P. Jain, J. Mudrich, and E. Popov. Parallel simulation of turbulent flows using lattice boltzmann models. In *American Nuclear Society Winter Meeting*, San Diego, CA, 2012.

[20] Chen S., Martinez D., and Mei R. On boundary conditions in lattice boltzmann methods. *Phys Fluids*, 8:2527–2536, 1996.

[21] H.J. Vogel, J. Tolke, V.P. Schulz, M. Krafczyk, and K. Roth. Comparison of a lattice-boltzmann model, a full-morphology model, and a pore network model for determining capillary pressure-saturation relationships. *Vadose Zone Journal*, 4(2):380–388, 2005.

[22] P. L. Bhatnagar, E. P. Gross, and M. Krook. A model for collision processes in gases. i. small amplitude processes in charged and neutral one-component systems. *Physical Review*, 94(3):511–525, 1954.

[23] D. D'Humieres, I. Ginzburg, M. Krafczyk, P. Lallemand, and L.S. Luo. Multiple-relaxation-time lattice boltzmann models in three dimensions. *Royal Society*, 360:437–451, 2002.

[24] M. Sukop and D. Thorne Jr. *Lattice Boltzmann Modeling: An Introduction for Geoscientists and Engineers*. Springer, 2006.

[25] L.V. Kantorovich and V.I. Krylov. Approximate methods of higher analysis. *Interscience Publishers*, 1958.

[26] V.L. Rvachev. Theory of r-functions and some applications. *Naukova Dumka*, 1982.

[27] V.L. Rvachev, T.I. Sheiko, V. Shapiro, and I. Tsukanov. On completeness of rfm solution structures. *Computational Mechanics*, 25:305–316, 2000.

[28] V. Shapiro and I. Tsukanov. Implicit functions with guaranteed differential properties. In *Fifth ACM Symposium on Solid Modeling and Applications*, Ann Arbor, MI, 1999.

[29] I. Tsukanov and V. Shapiro. The architecture of sagea meshfree system based on rfm. *Engineering with Computers*, 18(4):295–311, 2002.